Thesis for the degree of Licentiate of Engineering
in
Machine and Vehicle Systems

On power loss minimisation for heavy vehicles with axle-wise and modular electrical propulsion and friction braking

Sachin Janardhanan

Department of Mechanics and Maritime Sciences
CHALMERS UNIVERSITY OF TECHNOLOGY
Göteborg, Sweden 2023

On power loss minimisation for heavy vehicles with axle-wise and modular electrical propulsion and friction braking

Sachin Janardhanan

Thesis of Licentiate of Engineering 2023:03

Department of Mechanics and Maritime Sciences
Chalmers University of Technology
SE–412 96 Göteborg
Sweden
Telephone: +46 (0)31–772 1000

Chalmers Reproservice
Göteborg, Sweden 2023

On power loss minimisation for heavy vehicles with axle-wise and modular electrical propulsion and friction braking

Sachin Janardhanan
Department of Mechanics and Maritime Sciences
Chalmers University of Technology

Abstract

The main challenges for battery electric heavy vehicles are improving the payload capacity and driving range for different applications. These are mainly influenced because of battery power density, different vehicle configurations, and powertrain design. Therefore, a unique powertrain design for various vehicle configurations leads to a compromised driving range. Exploiting the features of the number of driven wheels and cost-neutral scalability of the electric machines adds to the over-actuation and provides opportunities to minimise the power losses.

In this thesis, to explore the potential of minimising the power losses, two powertrain topologies are analysed, namely, single e-axle group and multiple e-axle group. Additionally, a configuration of the multiple e-axle group called cruise and startability axles, with two different types of electric machines and gear ratios, is also presented. To coordinate the usage of actuators within these topologies, an algorithm that minimises the power losses of electric machines and friction brakes, while considering axle force limits, is introduced.

The power loss minimisation algorithm is then evaluated for a vehicle configuration using inputs, representing real-world operating points. The results show that the axle force limits introduced as constraints in the algorithm, influence the power loss minimisation potential of the topologies. For the inputs under study, the single e-axle group uses a large proportion of friction brakes instead of regenerative braking, resulting in high losses. Furthermore, it is shown that using multiple e-axle group topology with power loss minimisation increases the regeneration capabilities and vehicle performance.

Keywords: Heavy vehicles, powertrain, power loss, electric machines, friction brakes, topology

Acknowledgments

The research performed in this thesis was financially supported by Volvo Group Trucks Technology and Energimyndigheten under FFI program. I gratefully acknowledge this support.

I express my sincere gratitude to my supervisors Prof. Bengt Jacobson, Dr. Mats Jonasson and Adj.Prof. Leo Laine; for the motivation, encouragement and patience. Bengt with your insightful comments, enthusiasm and questioning the minute details, I feel none of my days were unproductive. Special thanks to Mats for the guidance, reviewing the quality of my work, valuable advice and discussions. Leo, thank you for the motivation, presenting the vision, creative ideas and being an excellent mentor. Thanks to Dr. Esteban Gelso for reviewing my work and articles with special mathematical stringency.

If not for the support and encouragement of my previous managers Stefan Edlund and Inge Johansson, this work would not have been possible. Thank you Sofi Sjögren, my current manager, for continuing the support, trust and discussions. Special thanks to the VEAS management and members for the support and helping me feel comfortable at the department. The Vehicle Analysis group; thank you for the interest shown in my work and encouragement from all of you. Thank you, Hiren Kerai, Sidhant Ray, Dr. Leon Henderson and Dr. José Vilca, for the support with preparations for the vehicle experiments. My room mate at VEAS, Umur Erdinc, appreciate your company for keeping both the academic and Volvo discussions ongoing. Thank you colleagues at VEAS: Luigi, Anandh, Erik, Johannes, Adam, Juliette, Arun, Björnborg, Avaneesh, Alexey and others, for like-minded discussions, lunch talks and of course Fika. Thank you Sonja, for taking care of all administration and making my life easy at Chalmers. Appreciate the support of those who I may have missed to mention.

Last but not the least, I want to thank my parents, family and friends for wishing me success and the constant support. Finally and most importantly, I thank Anuradha, my wife, for the support and patience extended during this work. Without your company, motivation and discussions, I would have struggled. Aryahi, your innocence and energy, help me connect to other part of life and keeps me going.

Thesis

This thesis comprises a summary and is based on the following appended papers:

Paper A
S. Janardhanan, L. Laine, M. Jonasson, B. Jacobson and M. Alaküla, *"Concept design of electric cruise and startability axles for long haul heavy vehicles to maximise driving range,"* 2021 IEEE Vehicle Power and Propulsion Conference (VPPC), Gijon, Spain, 2021, pp. 1-8, doi: 10.1109/VPPC53923.2021.9699364.

Paper B
S. Janardhanan, L. Laine, M. Jonasson, B. Jacobson and E. Gelso, *"Motion control and power coordination of electric propulsion and braking distributed on multiple axles on heavy vehicles,"* 2022 IEEE Vehicle Power and Propulsion Conference (VPPC), Merced, CA, USA, 2022, pp. 1-8, doi: 10.1109/VPPC55846.2022.10003450.

Paper C
S. Janardhanan, E. Gelso, L. Laine, M. Jonasson and B. Jacobson, *"Reviewing control allocation using quadratic programming for motion control and power coordination of battery electric vehicles,"* 2022 IEEE Vehicle Power and Propulsion Conference (VPPC), Merced, CA, USA, 2022, pp. 1-8, doi: 10.1109/VPPC55846.2022.10003297.

In addition, 3 patent applications in the area of motion control and power management have been filed directly as a result of this thesis.

Nomenclature

The nomenclature used here is applicable only for the thesis and not for the appended papers.

Symbols

$F_{x,req}$	Global longitudinal force request	N
$F_{y,req}$	Global lateral force request	N
$M_{z,req}$	Global yaw moment request	Nm
$F_{x,crs,req}$	Longitudinal cruise axle force request	N
$F_{x,crs,min}$	Minimum longitudinal force limit of the cruise axle	N
$F_{x,crs,max}$	Maximum longitudinal force limit of the cruise axle	N
$F_{x,stb,req}$	Longitudinal startability axle force request	N
$F_{x,stb,min}$	Minimum longitudinal force limit of the startability axle	N
$F_{x,stb,max}$	Maximum longitudinal force limit of the startability axle	N
$F_{x,brk,req}$	Longitudinal lumped friction brake force request	N
$F_{x,brk,min}$	Minimum longitudinal force limit of the lumped friction brake	N
$F_{x,brk,max}$	Maximum longitudinal force limit of the lumped friction brake	N
$F_{x,EMij,req}$	Longitudinal force request of the electric machine j on the axle i	N
$F_{x,EMij,min}$	Minimum longitudinal force limit of the electric machine j on the axle i	N
$F_{x,EMij,max}$	Maximum longitudinal force limit of the electric machine j on the axle i	N
$F_{x,brkij,req}$	Longitudinal force request of the friction brake j on the axle i	N
$F_{x,brkij,min}$	Minimum longitudinal force limit of the friction brake j on the axle i	N

$F_{x,brkij,max}$	Maximum longitudinal force limit of the friction brake j on the axle i	N
$F_{x,Axi}$	Longitudinal axle force on the axle i	N
$F_{y,Axi}$	Lateral axle force on the axle i	N
$F_{z,Axi}$	Vertical force on the axle i	N
$F_{x,Axi,lim}$	Longitudinal wheel force limit on the axle i	N
I_v	Inertia of vehicle around z-axis	$kg \cdot m^2$
l_f	Longitudinal position of the front axle from CoG	m
l_r	Longitudinal position of the rear axle from CoG	m
gr_{crs}	Cruise axle gear ratio	$-$
gr_{stb}	Startability axle gear ratio	$-$
$P_{loss,crs}$	Power loss of the cruise axle	kW
$P_{loss,stb}$	Power loss of the startability axle	kW
$P_{loss,brk}$	Power loss of the lumped friction brake	kW
$P_{loss,EMij}$	Power loss of the electric machine j on axle i	kW
$P_{loss,brkij}$	Power loss of the friction brake j on axle i	kW
r	wheel radius	m
$T_{x,crs,req}$	Cruise axle torque request	Nm
$T_{x,stb,req}$	Startability axle torque request	Nm
t	Vehicle track width	m
v_x	Longitudinal Vehicle speed	m/s
v_y	Lateral Vehicle speed	m/s
ω_z	Vehicle yaw rate	rad/s
w_{whl}	wheel speed	rad/s
φ_{ry}	Road gradient	rad

Definition

Topology Geometric arrangement of components in a vehicle layout. For example, the location of the electric machines, transmissions, and brakes mounted on the chassis connected to wheels.

Vehicle configuration Total number of wheels and the number of driven wheels. A pair of the driven wheels are usually on the same axle. For example, 4x2, 4x4, 6x4 etc.

Powertrain configuration Specification of the powertrain components, like gear ratio, EM power etc.

Acronyms

BEV	Battery electric heavy vehicle
TCO	Total cost of ownership
EM	Electric machine
PMSM	Permanent magnet synchronous machine
IM	Induction machine
CAN	Controller area network
DC	Direct current
QP	Quadratic Program
OP	Operating point
CoG	Centre of gravity
crs	Cruise axle
stb	Startability axle
brk	Friction brakes
whl	Wheel

Table of Contents

Chapter 1

Introduction

Demanding targets for CO_2 reduction have led to accelerated development and quick introduction of battery electric heavy vehicles (BEVs). However, due to the limitations in charging infrastructure and the energy density of batteries, the driving range and transportation time of BEVs are compromised. Therefore, every channel to extend the driving range needs to be explored. In particular the heavy vehicles, whose design and operation are usually mission-oriented, are also highly sensitive to the total cost of ownership (TCO). Hence, increasing the efficiency of the heavy vehicles and thereby driving range, is of primary importance to reach the targets of CO_2 reduction and keeping the TCO low.

1.1 Motivation

Heavy vehicles have been primarily built around diesel engines both from a geometrical and functional design perspective. Here, the geometrical design refers to the physical form and location of the prime movers, energy source, driver cabin, and layout of the axles. Similarly, the functional design here means the specifications defining the vehicle applications, for example long-haul, refuse, construction, and performance functionalities such as power transmission, braking, steering, and electronic control systems, etc. These geometrical and functional design requirements for heavy vehicles have been optimised over the years. Hence, due to the infrastructure built around diesel engines, the conventional heavy vehicle manufacturers configure electric powertrain based on the diesel engine-based vehicles [7][22]. Figure 1.1, shows an example of BEV based on the diesel engine based powertrain topology. This has introduced BEVs with an adaptation of the geometrical and functional designs primarily based on diesel engines. A typical example is the drive train used for a standard long-haul vehicle, where single or multiple rear axles are propelled using a shaft from the power source.

Electric machines for traction, unlike diesel engines offers features like high zero

Figure 1.1: Illustration of a 4x2 vehicle configuration, with chassis mounted prime mover and rear axle drive; (left): Historical diesel engine layout on Volvo ÖV4 TV pickup vehicle from 1927 [21]. (right): DAF LF Battery Electric Innovation Truck exhibited at IAA 2018 [7].

speed torque, regeneration capability, high power efficiency and wider speed and torque operation range [8]. Additionally, the power density (W/kg) of the electric machines is generally higher in comparison than diesel engines. These features influence two important vehicle development-based objectives: **a)** Scalability: since electrical machines, opposed to combustion engines, can in a cost-neutral way be divided into several smaller units. **b)** Packaging: Since electrical machines have a high power density and they are not very sensitive for mounting orientation and position, electric machines provide a freedom of packaging. Because of their operating range, the electric machines are usually configured without or with a transmission using single or fewer gears. This facilitates connecting of the electric machine directly to the wheel. Such a concept already existed in the 1900s, using wheel hub motors, as shown in figure 1.2. This prototype vehicle used four 2.5 to 3.5 hp hub-mounted electric motors that weighed around 1280 lbs totally. This vehicle also needed 1.8 tonnes of batteries with a capacity of around 270 Ah [15]. Although, the powertrain technology used in this vehicle was a revolutionary concept, it was too costly for the general population during that time. However, to meet the present operating demands by the heavy vehicles, axle-mounted electric machines have been introduced by the new heavy vehicle manufacturers such as Tesla and Nikola [11]. The electric machines are distributed on different axles, each with its own transmission system.

An additional challenge with heavy vehicles compared with passenger vehicles is the number of vehicle configurations, functional design system variants and powertrain topologies required for different applications. This poses additional

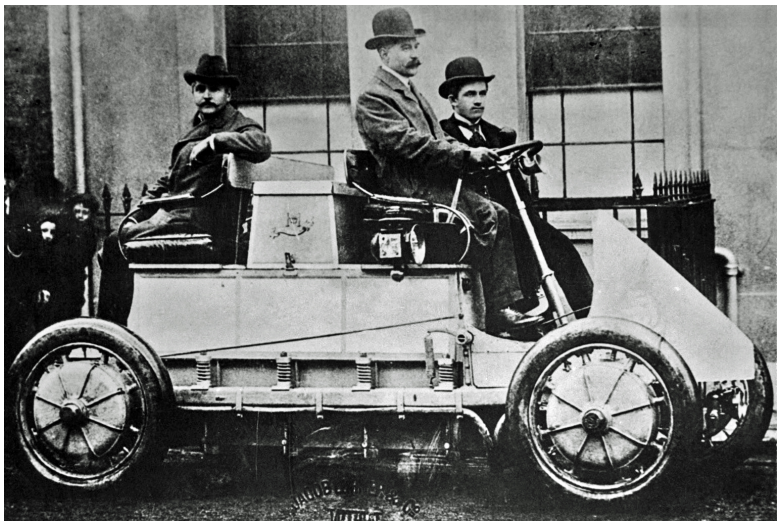

Figure 1.2: Lohner–Porsche Electromobile mixed hybrid using electric wheel hub motors [15]. Photograph from 1902.

requirements for the electric powertrain configuration and the connected energy efficiency. Heavy vehicles are also equipped with liftable axles, steered rear axle, and specific load carrying axles, which influence the powertrain topology and configuration. Thus, a unique powertrain solution does not cover the entire range of operation for specific applications. Hence, a modular and configurable approach is needed both from the physical and functional design perspective.

Profiting from the capabilities of electric machines in terms of regeneration, operating range, response time and installation flexibility, they can be blended with other actuators for stable vehicle behaviour and energy recuperation. This is known as over-actuation [14]. The degree of over-actuation is limited on diesel engine based topologies and configurations, owning to the slow dynamics of the system and the available actuation capabilities of the axles [1]. With electric machines distributed on several axles, the degree of over-actuation further increases and presents opportunities to improve energy efficiency as an example, by using machines at their best possible operating points. Different objectives such as minimising the wear of actuators, power consumption and equal friction utilisation of the wheels are other objectives that can be exploited. This added potential of the electric machines facilitates the use of integrated motion control and power management algorithms for actuator coordination with additional objectives such as safety, energy efficiency, among others.

Energy prices and battery energy densities influence the TCO of BEVs. Analysis of the current BEVs in [2], highlights that around one-third of TCO is associated with the energy costs. This is in addition to high initial investment cost, which has a significant influence on the BEV consumers. In contrast, it

is also not profitable for the manufacturers to customise vehicles exactly as per the requirements. This necessitates a balanced and modular approach for BEV development. In addition to the vehicle development-based improvements, research on effective route planning, utilisation, battery technology, and predictive energy strategies of electric vehicles to reduce the energy consumption are ongoing [3]. These are primarily performed on BEVs developed using diesel engine based topologies. Hence, one could also challenge if the current vehicle design is optimal for BEVs. For example, all the subsystems and components within, such as powertrain topology, suspension, steering, brakes etc., have been developed based on diesel engine based topologies over the years. Thus, in this thesis, the main aim is to identify the optimal powertrain topology for BEVs. The primary research focus is to minimise the energy consumption through optimisation of powertrain configuration for a given topology and identify the additional features. In [20], it is shown that by the choice of the topology along with the right configuration can result in 5.6% of TCO variation and that the distributed topology gives the lowest TCO. With propulsion distributed over multiple axles and using optimal axle coordination methods such as control allocation, there are possibilities to reduce instantaneous power losses. The relocation of prime movers on to the axles also provides opportunities to influence geometrical and functional vehicle design.

1.2 Research questions

The following research questions were investigated in this thesis:

- How should modular e-axle topologies be chosen to meet heavy vehicle requirements for cruise-, startability-, and power modes ?
- How to coordinate longitudinal motion actuators on each axle, minimising the power losses and achieving the desired longitudinal motion ?

1.3 Limitations

This scope in the thesis is limited :

- to the design of instantaneous control of the motion actuators and not any predictive control.
- by assuming that the upper functional layers of the hierarchical structure requests only motion requests, and no requests on which actuator to use or which axle or wheel to use.

- to energy consumption calculations using only heat losses produced by the electric machines and friction brakes. Energy losses in battery and auxiliary systems are not in cost function that is minimised. This means, e.g. that power losses in battery and of auxiliary equipment are not minimised.
- by not including studies on vehicle motion in the reverse direction and other close to standstill operating conditions.
- by not studying different wheel torque actuations on the left and right sides.

1.4 Contributions

The contributions from this thesis to the scientific community are the following:

- Introduction of the modular concept of separate cruise and startability e-axle, and parameter optimisation of electric machine power and gear ratios to increase driving range. - **Paper A**
- Evaluation of, and selection among, different methods of actuator coordination to minimise power losses while fulfilling motion request for powertrain topology with multiple axles. - **Paper B and C**
- A modular optimisation algorithm for axle coordination, using simplified formulation of combined slip, while minimising power losses. - **Thesis**
- Python-based code for power loss minimisation using actuator and axle coordination - `https://github.com/sachinj486/Powerlossmin-EM-and-brakes`

Chapter 2

Electric propulsion topologies on a vehicle unit

The electrification of the propulsion systems in BEVs has introduced numerous powertrain topologies and configurations. Fundamentally, the powertrain design involves the optimisation of the topology, hardware components and the control system. The choice of powertrain topology and configuration also influence the geometrical and functional design of the vehicle. In this chapter, two such electric powertrain topologies are introduced. In section 2.1, a topology based on the diesel vehicle design is introduced. Following which a topology with electric machines and transmissions located on multiple axles in section 2.2.

2.1 Single e-axle group

In this thesis, the single e-axle group topology means to follow the same geometrical and functional design as a traditional diesel engine, as shown in figure 2.1. This infers that all prime movers, here the electric machines, are located at a specific position on the chassis frame; transfer power to one shaft and then to the wheels through transmission, differentials, and drive shafts. Due to power requirements for heavy vehicle applications, a common approach is to use to three or four electric machines connected in parallel to the transmission system (c.f. multiple cylinders in a diesel engine). The number of machines and the design of the transmission depends on the physical size and specifications of the EM. Functionally, to propel or decelerate the vehicle all the electric machines are forced to operate together due to one single shaft before transmission.

Furthermore, the mechanical components for power transmission such as gears and differentials are, also associated with load dependent and load independent losses. These mechanical systems and components also limit the available pack-

aging space for the batteries and other electrical systems. The batteries used for electric propulsion are usually connected together electrically and act as a single energy source. For a standard long-haul vehicle with this topology, means that all the propelling and regeneration is primarily limited to the rear axle or axle group. This capability depends on the load on the axle, tyre-road friction, and actuator operating limits. Additionally, all the wheels are equipped with friction brakes to meet the high deceleration requirements whenever required. The use of mechanical clutches is important in reducing the idle losses of the PMSMs, but they lead to extra hardware and increased cost of the powertrain system [10][19].

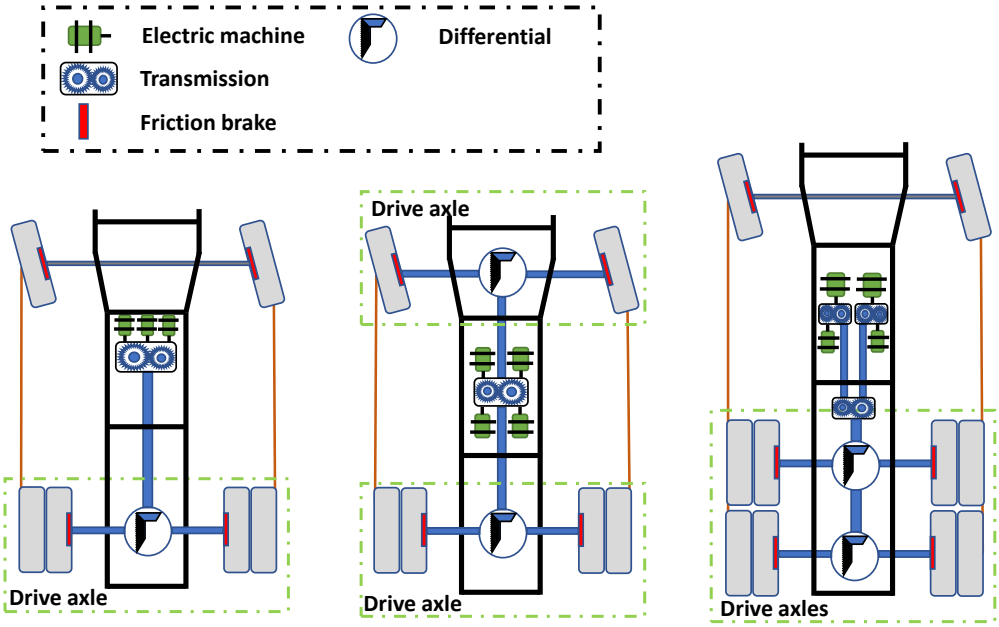

Figure 2.1: Examples of single e-axle group topologies on different vehicle configurations; (left): 4x2; (Center): 4x4 (right): 6x4.

2.1.1 Discrete machine usage

An alternative method to reduce the idle losses of IMs is to de-energise them. This feature is specific to IMs as both the stator and rotor magnetic fields are generated using the same supply current. To verify this feature, a preliminary investigation was performed on a single e-axle group topology, with real vehicle tests. The vehicle as shown in Figure 2.2, is configured with four IMs along with inverters, which all drive a common shaft. The inverter software was also programmed with a specialised interface, giving individual control to each machine with the capability to switch on/off each inverter. The specialised software interface also

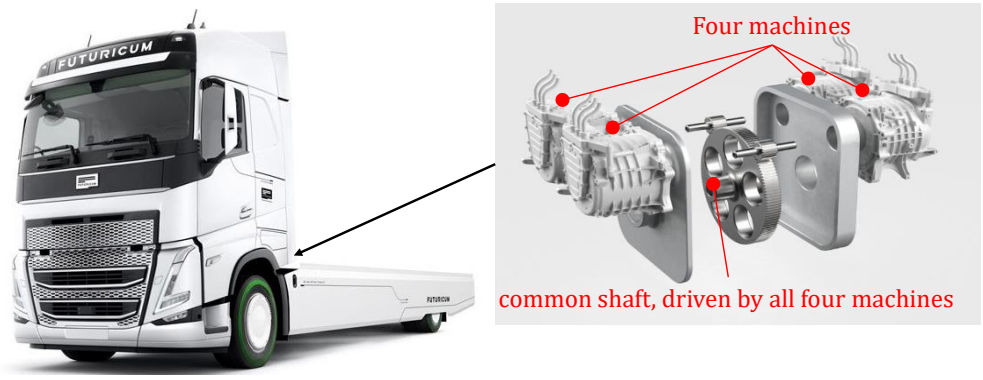

Figure 2.2: Layout of IMs on a 4x2 tractor with specialised interface for discrete machine usage [16].

relayed individual actuator signals and statuses. The necessary signals such as machine voltage, torque output, and machine speed were available on vehicle CAN [13]. To measure the DC current, clamp sensors [6] were used on cables connecting the high-voltage battery to the individual inverters.

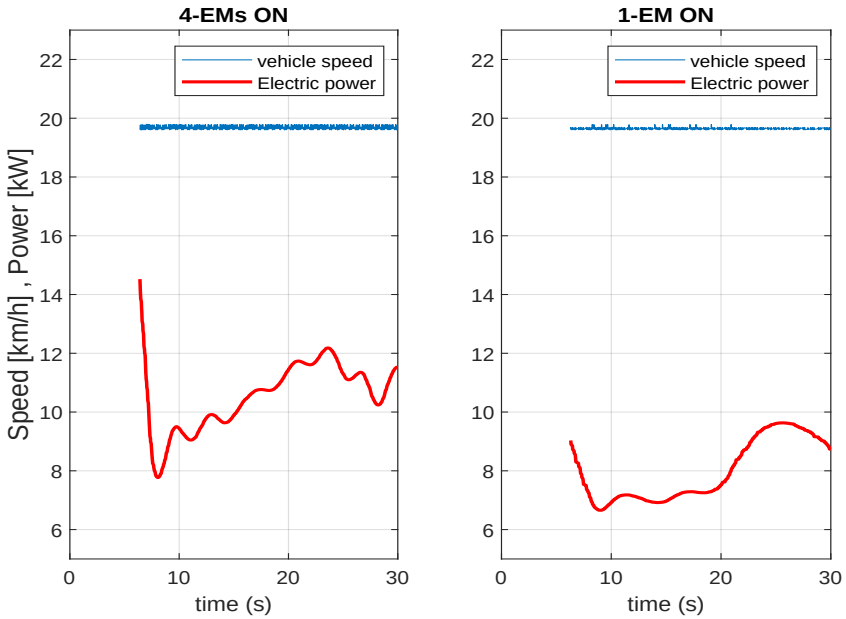

Figure 2.3: Results from real vehicle measurements. The electric power consumption are evaluated for the case using 4 EMs and 1EM, for the same vehicle operating conditions.

A series of test runs were performed, using 4 EMs followed by switching off 3 machines and evaluating the input and output power at the EMs. Post processed

test results are plotted in figure 2.3. Comparisons of electric power consumption, was done for the same vehicle motion. The tests indicated that there are vehicle operating conditions where one can reduce power losses by switching off some machines. However, more analysis and investigation is needed, so the author chose to not lift these preliminary results as a contribution to the thesis. It might be a future work to develop control algorithms that utilises the possibility to switch off single machines in vehicles where one have multiple machines.

2.2 Multiple e-axle group

In this thesis, the multiple e-axle topology means to follow a different geometrical and functional design compared to a traditional diesel engine vehicle, as shown in figure 2.1. The power sources are distributed among axles compared with the single e-axle topology, where the power source is centralised and mounted on the chassis frame. These axles are assumed to be individually propelled and not physically coupled [5]. For example, this configuration could be two driven axles on a 4x4 vehicle or two rear driven axles in a 6x4 vehicle with the front axle being steered and non-driven. The axles in multiple topology could be configured with single or multiple electric machines and transmission placed on each axle. This topology is expected to give more packaging space, reduced losses and possibility to have a better design of a driver cabin.

2.2.1 Cruise and startability axles

The cruise and startability axles are conceptualised as a distributed topology and configured with electric machines and gears on the specified axles. In this thesis, only one electric machine and gear ratio are configured on each axle, however multiple machines and gear ratios are also possible. A special variant of multiple machines could be one that allows torque differentiation between the left and right sides. Figure 2.4, shows examples of arrangement of cruise and startability axles on two different vehicle configurations, but not limited to these arrangements. A comparable topology is also recently seen on the latest Tesla semi [11]. However, the types, the configuration of the machines, and gear ratios are not found in the public domain.

As indicated by the naming "cruise and startability axles", each axle is specifically designed for a particular operating mode of the vehicle; the cruise axle, both the electric machine and gear ratio, is primarily dimensioned for cruise mode operations and the startability axle for startability mode operations. Here, the dimensions of the EMs refer to the maximum continuous power and rotating speeds. Both the axles are designed to operate independently or in combination

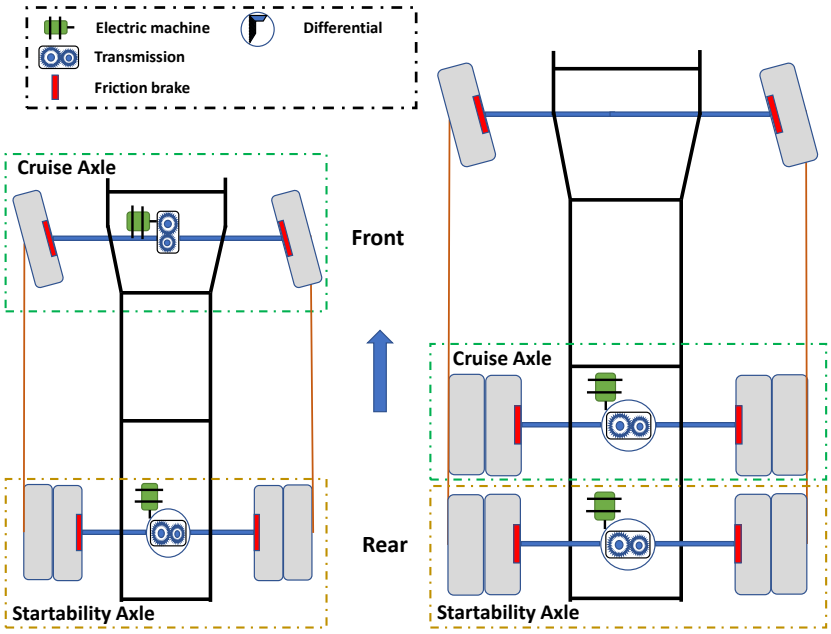

Figure 2.4: Examples of arrangement of cruise and startability axles; (left): 4x4 tractor; (right): 6x4 tractor. The transmission system here assumes the differential function on each axle.

over the entire vehicle operating range. In this thesis, the cruise mode is defined as the operation of a vehicle at cruising speeds, for example, 80 km/h with a maximum grade of $\pm 2.5\%$ assuming flat road conditions (T-FLAT) [18]. The cruise axle then must be dimensioned to operate efficiently for cruise mode operations. Similarly, the startability mode is defined as the vehicle start or take-off operations on grades higher than a target startability grade, as an example around 8% uphill. The startability axle should be dimensioned based on the startability mode requirements and able to deliver continuous torque. The startability mode requires high torque and transient operations from the electric machines.

However, for the entire vehicle operations, these two distinct modes are not sufficient. The acceleration performance of the vehicle over the entire operating range also needs to be considered, while setting requirements for the powertrain configuration. For example, in Paper A, an maximum acceleration requirement of 0-80 km/h in less than 46 s is applied. Due to the cooling system design, efficiency considerations, and transient high operating demands, axles may not be able to fulfill the operating requirements individually. A vehicle mode where both axles supply power is referred to as the power mode. In situations, such as acceleration during, take-off at high grades, for example road grades above 10%, or overtaking at high speed, additional power and torque is needed.

Therefore, all the requirement of the three modes must be utilised in specifying the powertrain configuration. A simplified illustration of the different operating modes is shown in figure 2.5, using the force-vehicle speed diagram. These modes can be configured as a specific target or target range and adapted based on the vehicle application. Also, the name classification is not unique and can be set according to different operating conditions.

In this thesis, the cruise axle is configured with a PMSM, having high efficiency, torque density, and continuous power delivery. This configuration assumes that the long-haul vehicle is used $> 90\%$ of the operating time in a cruise mode. Therefore, this allows to accommodate a relatively lower efficient EM on the startability axle, as it is operated intermittently and for short duration while accelerating and taking-off from a standstill. Thus, to complement the PMSM, the startability axle is configured with an IM, which is cheap, robust and easy to maintain. The utilisation of PMSM and IM machines on cruise and startability axles, respectively, is expected to give a balance of cost, performance, and efficiency. Hence, depending on the vehicle application demands, different types of machines and their configurations need to be explored. The torque speed maps of the cruise axle, PMSM, and startability axle, IM, used for the coordination is presented in figure 2.6. Furthermore, IMs can also be de-energised, an alternative to using a mechanical clutch, as shown in (2.1.1), and thereby reducing the idle losses. Nevertheless, the influence of de-energising or the use of mechanical clutch is not further explored in this thesis.

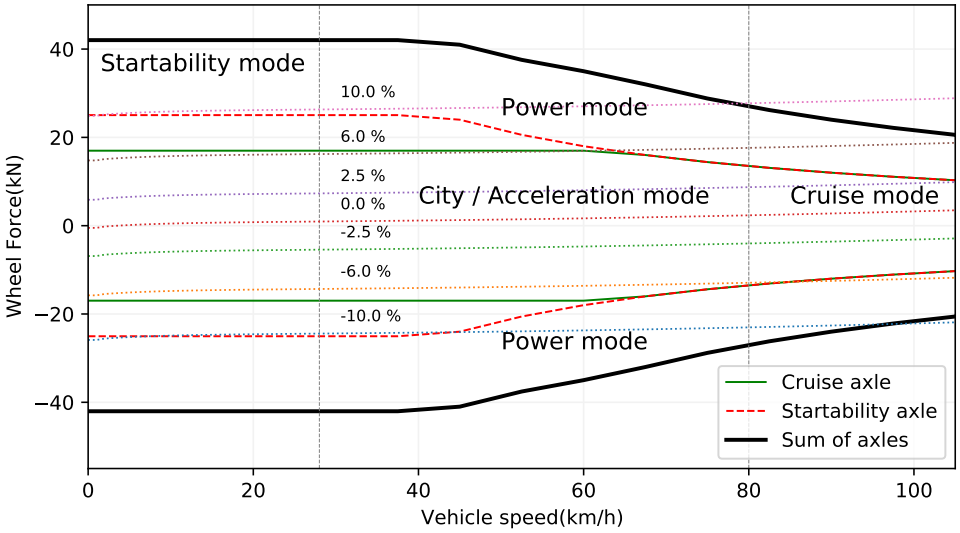

Figure 2.5: A simplified representation of the different vehicle operating modes used to configure the cruise and startability axles, visualised on a wheel force and vehicle speed diagram.

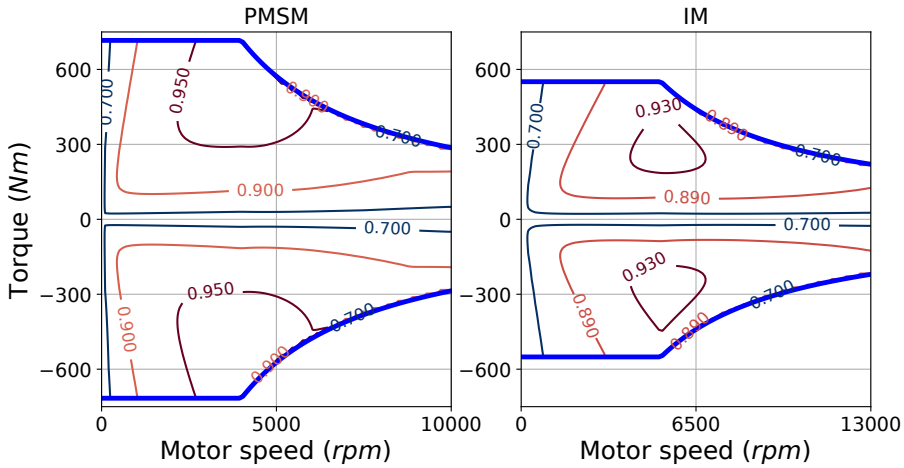

Figure 2.6: Torque-speed map of electric machine from a model used for power losses. (left): $300kW$, PMSM ; (right): $300kW$, IM. Efficiencies are expressed as a function of torque and speed and represented as contours (labeled contour lines with efficiencies within the blue lines) and the torque limit ($T_{j,lim}$ where $j = crs, stb$), represented by thick blue line for each machine.

Additionally to improve the range, the cruise and startability e-axles also require momentaneous control in addition to the optimal configuration for a given driving cycle, from human pedal driving or from a predictive cruise control. Since, this topology is over-actuated , there are multiple ways to achieve the required motion request. In Paper A, an example of how to control e-axles is also presented, based on an optimisation-based control allocation [17] [4]. Furthermore, a method to optimise the powertrain configuration parameters of cruise and startability axles is proposed.

Chapter 3

Actuator coordination

With the introduction of integrated vehicle control systems, a combination of actuator systems can perform a task that used to be performed by a specific actuator system. This is also referred as over-actuation and represents an redundant system; which means there are lesser degrees of freedom to influence than the total actuator combinations to control them. Mathematically, such an under-determined system of equations can be solved using control allocation. Control allocation, in principle separates the actuator selection task from the actual control of the actuators. This chapter presents two optimisation-based control allocation methods. In section 3.1, the problem of over-actuation in the longitudinal direction for the multiple e-axle group is introduced. Section 3.2 presents the power loss minimisation method used for actuator coordination followed by the weighted optimisation method in section 3.3.

3.1 Over-actuated in longitudinal direction

Road vehicles are usually configured with different actuator systems that have specific objectives. For example, the brake system should be able to hold the vehicle on a hill and cover the range of retardation requirements. Similarly the propulsion system should be able to provide constant power at high speeds and accelerate the vehicle from low speeds. With the introduction of an electric propulsion system, there is a possibility of performing functions of braking and steering in addition to propelling. The rate and range of braking and steering performance using electric machines however is limited and depends on the vehicle configuration. This allows the actuator requests to be distributed among the actuators optimally fulfilling some objectives. The common objectives usually minimised are the usage of actuators, tyre or actuator wear, energy and power loss.

For the single e-axle group using a single machine or multiple machines of the same configuration and by excluding the coordination of the axles, the actuator

coordination is trivial for longitudinal motion. The rational solution is to use the electric machines both for propulsion and braking to the maximum and then add friction brakes in case of additional retardation. However, when multiple EM's of different configurations are used on single e-axle group topology and axle wise friction brakes are combined, the system becomes over-actuated with non-trivial solutions already in the longitudinal direction. This is also the same case with the multiple e-axle group topology. For instance, a vehicle with a cruise axle, startability axle, and friction brakes, the requested longitudinal force $F_{x,req}$, to fulfill the required motion, is achieved using all the three actuator types:

$$F_{x,req} = F_{x,crs,req} + F_{x,stb,req} + F_{x,brk,req} \tag{3.1}$$

where the $F_{x,crs,req}$ is the cruise axle force request, $F_{x,stb,req}$ is the startability axle force request, and $F_{x,brk,req}$ is the total lumped friction brake force request to the friction brakes. The wheel forces on the cruise and startability axle due to electric machines are also lumped to one force per axle. Although the real request to the actuators is torque, in this thesis only force request is imagined as the output of the actuator coordinator. This is by assuming that there is a final step that is not included in the actuator coordination algorithm, in which force is converted to torque.

$$F_{x,req} = \frac{T_{x,crs,req}}{r} + \frac{T_{x,stb,req}}{r} + \frac{T_{x,brk,req}}{r} \tag{3.2}$$

Additionally, there are several ways to set up an optimisation formulation as a control allocation problem. In papers B and C, two different methods are elaborated. In the next section 3.2, the objective approach of using physical models of power loss for cruise and startability axles concept as an optimisation formulation is shown. This is followed by a method involving solving of an multi-objective optimisation formulation called the weighted optimisation formulation in section 3.3.

3.2 Power loss minimisation by actuator coordination

In this approach, the main aim is to minimise instantaneous power losses from electric machines and friction brakes, while achieving the longitudinal force request, $F_{x,req}$. Since, the significant proportion of power losses origin from the electric machines and friction brakes as shown in [19], other sources of losses like tyre slip, rolling resistance, etc., are excluded. Furthermore, only losses that are converted to heat by the electric machines and brakes, are minimised. The vehicle representation used in the actuator coordinator is simplified to a single lumped

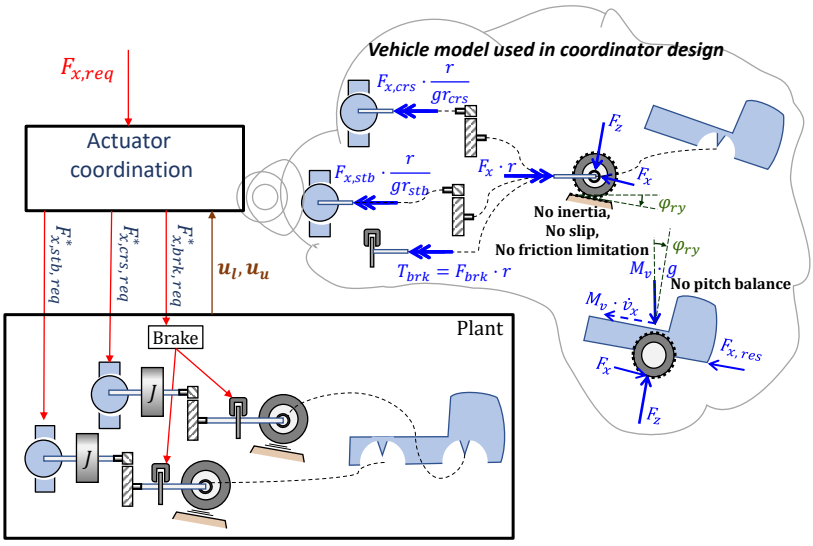

Figure 3.1: Simplified view of the actuator coordination process. The vehicle representation as a lumped mass and one wheel model used in actuator coordination is also highlighted.

mass with one wheel, as shown in figure 3.1. Additional effects of inertia, slip and friction limitation on the wheel are also not included.

The actuator coordination problem is expressed as an optimisation formulation solving for optimal actuator requests, $\boldsymbol{u^*} = [F^*_{x,crs,req}, F^*_{x,stb,req}, F^*_{x,brk,req}]^T$:

$$\begin{aligned} \boldsymbol{u^*} &= \arg\min_{\boldsymbol{u}} \left(\sum P_{loss,j}(\boldsymbol{u}) \right) \\ &\text{s.t} \quad B\boldsymbol{u} = \boldsymbol{v} \\ &\qquad \boldsymbol{u_l} \leq \boldsymbol{u} \leq \boldsymbol{u_u} \\ &\text{where, } j = \{crs, stb, brk\} \\ &\boldsymbol{u_u} = [F_{x,crs,max}, F_{x,stb,max}, F_{x,brk,max}]^T \\ &\boldsymbol{u_l} = [F_{x,crs,min}, F_{x,stb,min}, F_{x,brk,min}]^T \end{aligned} \tag{3.3}$$

From (3.3), $P_{loss,crs}$ is defined as the cruise axle power loss, $P_{loss,stb}$ as the startability axle power loss, and $P_{loss,brk}$ the power loss of the lumped friction brake. The term, $\boldsymbol{v} = F_{x,req}$, represents the global longitudinal force request and B is called the control effectiveness matrix. In the consideration, that both $\boldsymbol{v}$ and $\boldsymbol{u^*}$ are force requests, B essentially becomes a vector of ones, for example, in this case $B = [1, 1, 1]$. The terms $\boldsymbol{u_l}$ and $\boldsymbol{u_u}$, are the vectors of actuator limits, obtained using minimum and maximum torque limits, at a given operating speed, v_x, respectively. The elements of the $\boldsymbol{u_l}$ and $\boldsymbol{u_u}$, can be obtained as shown in (3.4) and (3.5), where $T_{j,lim}$ is obtained from the EM model as shown in figure 2.6 and

$T_{brk,lim} = 80kNm$.

$$F_{x,j,min} = \begin{cases} \min(T_{j,lim}(\frac{v_x \cdot gr_j}{r})), & \text{if, } j = crs, stb \\ \frac{-T_{brk,lim}}{r}, & \text{otherwise} \end{cases} \tag{3.4}$$

$$F_{x,j,max} = \begin{cases} \max(T_{j,lim}(\frac{v_x \cdot gr_j}{r})), & \text{if, } j = crs, stb \\ 0, & \text{otherwise} \end{cases} \tag{3.5}$$

In cases, when $B\boldsymbol{u} = \boldsymbol{v}$ cannot be fulfilled due to $\boldsymbol{u_l}$ and $\boldsymbol{u_u}$, the aim is to have a solution that gives the smallest difference $|B\boldsymbol{u} - \boldsymbol{v}|$. In most cases, and cases studied in this thesis, this is managed by saturating the incoming request $\boldsymbol{v}$ before the optimisation. Therefore, $B\boldsymbol{u} = \boldsymbol{v}$ is always considered as possible to fulfilled.

3.2.1 Electric machine losses

Electric powertrains have losses in battery, power transmission cables, inverters, electric machines and transmission etc. However, for the actuator coordination related optimisation, only the electric machines and inverter are considered. Inverters have losses due to heating of electrical components such as resistors and capacitors. Whereas in the electric machines losses are due to heating up windings, magnetic losses in windings and core and frictional losses.

In Paper B, the losses of electric machines and inverter are extracted using a physical model expressed as a function of torque and speed. The power losses for each machine, as a function of its torque, for different vehicle speeds are seen in figure 3.2. Note that the capabilities are also visualised by the end of the curves. A quadratic regression model also presents the power loss characteristics for the entire torque with acceptable accuracy for most of the machines and can be expressed as:

$$P_{loss,j} \approx a_j \cdot T_j^2 + b_j \cdot T_j + c_j, \tag{3.6}$$

where, a_j, b_j and c_j - curve fitting coefficients; $j = crs, stb$

Furthermore, the power loss model can also be extracted using measurements and expressed as a look up table as shown in [19]. The coefficients of regression polynomial are used to describe the power loss characteristics.

3.2.2 Friction brake losses

Any usage of friction brakes, due to friction between the brake pad and the disc, results in 100% loss as heat. The power losses from the friction brakes, can be

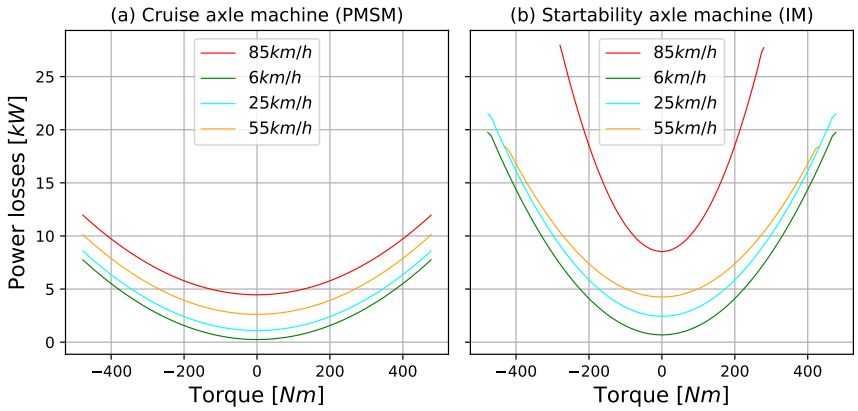

Figure 3.2: Power losses of electric machines as a function of torque for different vehicle speeds. The offset of power losses at zero torque is referred to as idle losses which is higher at higher speeds.

expressed as a linear relation of mechanical power:

$$P_{loss,brk} = -T_{brk} \cdot \omega_{whl}, \text{where } \omega_{whl} \text{ is the wheel speed.} \tag{3.7}$$

Other forms of losses due to the air compressor operation and leakage are not considered as they are small in magnitude compared to heat losses due to brake mechanism actuation.

3.2.3 Optimisation using quadratic programming

Referring to the loss functions in (3.6) and (3.7), it is noticed that the highest order of the power losses associated with the actuators is quadratic. The quadratic nature of the loss functions and use of linear constraints in (3.3), represents a convex problem and hence a global minimum is assured. The minimisation problem can be solved using quadratic programming and the power loss minimisation formulation in (3.3) is reformulated, solving for $\boldsymbol{u}^*$:

$$\begin{aligned} \boldsymbol{u}^* &= \arg\min_{\boldsymbol{u}} \quad \frac{1}{2}\boldsymbol{u}^T H \boldsymbol{u} + g^T \boldsymbol{u} \\ \text{s.t.} \quad & B \cdot \boldsymbol{u} = \boldsymbol{v} \\ & \boldsymbol{u}_l \leq \boldsymbol{u} \leq \boldsymbol{u}_u \\ \text{where} \quad H &= 2 \cdot \begin{bmatrix} \frac{r^2}{gr_{crs}^2} \cdot a_{crs} & 0 & 0 \\ 0 & \frac{r^2}{gr_{stb}^2} \cdot a_{stb} & 0 \\ 0 & 0 & a_{brk} \end{bmatrix} \end{aligned} \tag{3.8}$$

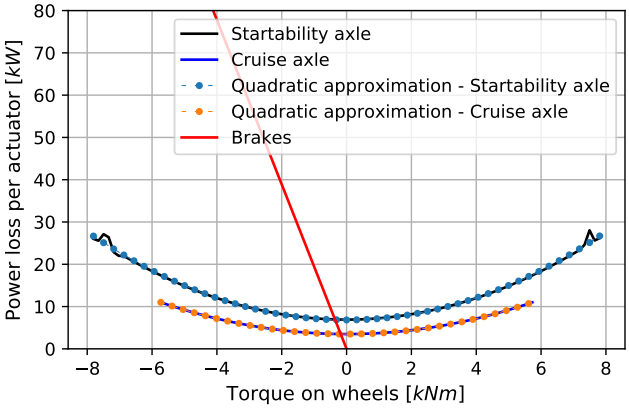

Figure 3.3: Power losses of electric machines with their quadratic approximations and friction brakes, as a function of wheel torque for a vehicle speed of 70 km/h. The curve fit parameters for the regressed quadratic approximations of: **a)** cruise axle electric machine - $a_{crs} = 0.033, b_{crs} = -0.0002, c_{crs} = 3498.44$ giving an $R2$ fit of 0.99 **b)** Startability axle electric machine - $a_{stb} = 0.17, b_{stb} = 0.038, c_{stb} = 6838.84$ giving an $R2$ fit of 0.99.

$$g^T = \left[\frac{r}{gr_{crs}} \cdot b_{crs}, \frac{r}{gr_{stb}} \cdot b_{stb}, -\omega_{whl} \cdot r\right]$$

Figure 3.3, shows the power losses of each actuator, as a function of wheel torque for a certain vehicle speed. Note that the electric machine losses and torques are scaled as wheel losses and torques respectively.

Hence, the function of the actuator coordinator, while minimising the power losses, is to select one point on each curve. The sum of the three torque requests achieves the total wheel torque requested ($F_{x,req} \cdot r$). Mathematical manipulations were performed in Paper B to solve the quadratic programming problem. For example, a numerically small value, $a_{brk} = 1e^{-5}$, is used as the coefficient of the quadratic term for the friction brakes to ensure that the hessian is positive semi-definite. Furthermore, only positive values of $F^*_{x,brk,req}$ are used in (3.8). To include the driving conditions representing near standstill and reversing, some manipulations are needed, which are not covered in this thesis.

3.3 Weighted optimisation method

An alternative approach, to solve the actuator coordination task is solving a two-step sequential optimisation problem with l_2 norm [9].

$$\begin{aligned} \boldsymbol{\Omega} &= \arg \min_{\boldsymbol{u_l} \leq \boldsymbol{u} \leq \boldsymbol{u_u}} (\|W_u(B\boldsymbol{u} - \boldsymbol{v})\|_2^2) \\ \boldsymbol{u^*} &= \arg \min_{\boldsymbol{u} \in \boldsymbol{\Omega}} (\|W_u(\boldsymbol{u_{des}} - \boldsymbol{u})\|_2^2) \end{aligned} \tag{3.9}$$

The most commonly employed method to solve the sequential optimisation problem in 3.9 is by adding a weighting term γ and solve it in one step, as shown in 3.10.

$$\begin{aligned} \boldsymbol{u}^* &= \arg\min(\|W_u(\boldsymbol{u_{des}} - \boldsymbol{u})\|_2^2 + \gamma\|W_v(B\boldsymbol{u} - \boldsymbol{v})\|_2^2) \\ \text{s.t.} \quad & \boldsymbol{u_l} \leq \boldsymbol{u} \leq \boldsymbol{u_u}, \quad \boldsymbol{u_{des}} = [0,0,0]^T \end{aligned} \tag{3.10}$$

The weighted optimisation is referred to as global force minimisation in Paper B since the global force request error term $\|W_v(B\boldsymbol{u} - \boldsymbol{v})\|$ is heavily weighted, which means also highly prioritised. This formulation is thoroughly analysed numerically in Paper C and referred to as a mixed optimisation formulation. Similar to power loss minimisation, this method is solved using QP solvers, and how to convert the problem formulation into the QP form is seen in appendix A. In comparison with power loss minimisation, this method solves a multi-objective cost function prioritising the motion objective while ensuring minimal actuation of actuators, as shown in (3.10). Here, minimal actuation means to reduce the amplitude of the actuator operation from its reference state also represents power loss. This is assuming that the zero state is the equilibrium state consuming least power. Furthermore, as seen in (3.10), the global force error is minimised only as compared to achieving the global force with an equality constraint in the power loss minimisation scheme. The global force minimisation method needs

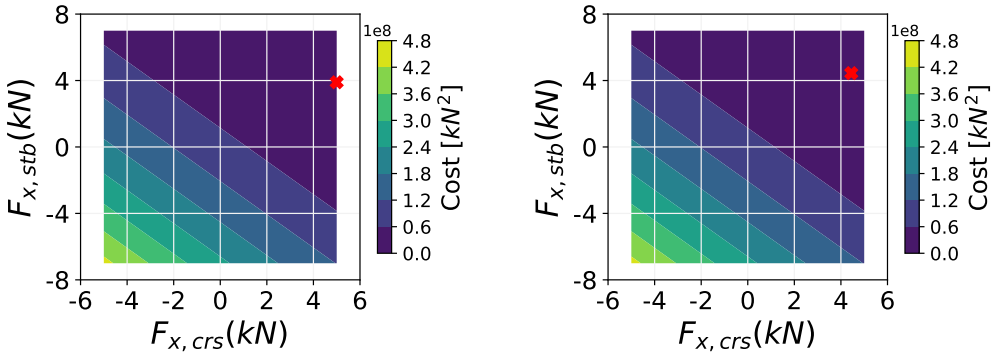

Figure 3.4: Influence of W_u values on force allocation with $u_{des} = [0;0]$, $\boldsymbol{v} = 8895N$, $\boldsymbol{u_l} = [-5000,-7000]$,$\boldsymbol{u_u} = [5000,7000]$ and with $B = [1,1]$ and $W_v = 1$. The X and Y axis in the plots represents the range of force allocation possible for the cruise and startability axle respectively. The cost of the entire solution space, represented by the contours, is achieved by solving the cost function in (3.10) at each point on the X and Y axis. Optimal solutions are represented by the red cross marker for each of the following configuration of W_u and γ used: (a):$W_u = diag(10^{-5}, 10^{-2})$, $\gamma = 10^2$; (b): $W_u = diag(1,1)$, $\gamma = 10^2$

inputs of u_{des} and W_u. Exactly how to calculate those is not in the scope of the thesis, but [14] claims that they can be calculated using values from previous time

instants and heuristics. For example, in Paper B and C, it is assumed that the PMSM operation on the cruise axle is always optimal and should be prioritised. Hence, the PMSM is always used to the maximum and only for requests above the limits of the PMSM, the startability is supplemented followed by brakes. This is achieved by the tuning vector W_u and requires some effort. An example of the effect of tuning W_u, on the coordination of cruise and startability axle force, is seen in figure 3.4.

In Paper C, the influence of different tuning factors and constraints on the actuator coordination is presented. Additionally, the metrics used to evaluate the solutions are highlighted. With the multiple actuators weighted optimisation method becomes tedious and invalid for all operating conditions for the vehicle. Hence, the weighted optimisation method will not be used for further analysis in this thesis.

Chapter 4

Adding axle coordination

The vehicle motion control means achieving the requested forces and moments from the tyres, in the road plane. Usually a controller from an upper functional layer in a hierarchical structure sends requests as inputs from a human driver or from automatic driving algorithms. These required forces and moments are produced by the actuators and are transmitted to the wheels. In this chapter, the actuator coordination presented in the previous chapter, is extended by also considering vehicle dynamics . Axle loads, road friction and vehicle manoeuvre restrict the amount of requested force that is actually available at the wheel to produce the requested forces and moments.

4.1 Over-actuation in longitudinal and lateral direction

In the road plane, the vehicle has a lateral and yaw degree of freedom in addition to the longitudinal motion. With the assumptions of negligible, vertical dynamics, pitch, and roll movements, these motions are represented using a vehicle model as seen in (4.1) and figure 4.1.

$$\begin{aligned} M_v \cdot (\dot{v}_x - v_y \cdot \omega_z) &= F_{x,c1} + F_{x,c2} + F_{x,c3} + F_{x,c4} \approx F_{x,req} \\ M_v \cdot (\dot{v}_y - v_x \cdot \omega_z) &= F_{y,c1} + F_{y,c2} + F_{y,c3} + F_{y,c4} \approx F_{y,req} \\ I_v \cdot \dot{\omega}_z &= -F_{x,c1} \cdot t/2 + F_{x,c2} \cdot t/2 - F_{x,c3} \cdot t/2 + F_{x,c4} \cdot t/2 \\ &\quad + F_{y,c1} \cdot l_f + F_{y,c2} \cdot l_f - F_{y,c3} \cdot l_r - F_{y,c4} \cdot l_r \approx M_{z,req} \end{aligned} \tag{4.1}$$

To achieve the desired motion, a controller calculates the global force and moment requests, $[F_{x,req}, F_{y,req}, M_{z,req}]^T$, using the driver inputs[14]. How to calculate the total force request in the longitudinal direction, from the controller is shown in

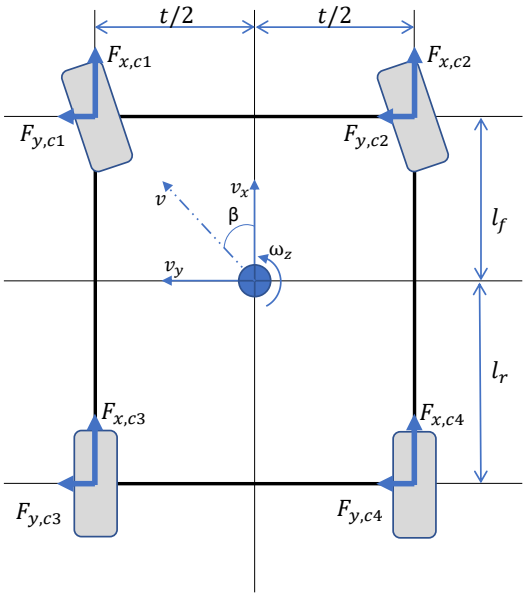

Figure 4.1: Two track vehicle model in the road plane having longitudinal, lateral and yaw rotational degree of freedom.

Appendix B. The respective actuators then produce the desired wheel forces, following the request, overcoming the resistances and losses.

Furthermore, these motions are not independent of each other. Due to the tyre characteristics, the lateral forces on the vehicle limit the longitudinal force available and vice versa. Hence, these effects need to be included while preparing the request in the controller, as shown in [12]. Adding, such details in the controller lead to complexity in modelling, tuning, and deviations in results due to estimation. In the next section, a method to implement such effects as constraints to an optimisation formulation is presented. This results in an independent and modular actuator coordination algorithm without dependency on the controller.

4.2 Adding axle constraints to fulfill axle level coordination

The effects of tyre characteristics on the actuator coordination are introduced as constraints in the optimisation formulation. An effective way to include these effects is by using friction circle representation of the wheel forces. In this thesis, in addition to the introduction of these effects, the following simplifications are made:

- assuming that there is no lateral load transfer between the wheels and hence

lumping them into lateral force per axle. This is what is often called a one-track model.

- limiting the actuator sets to electric machines and brakes, which can influence the vehicle motion.

Also assuming only quasi-steady state cornering conditions, the vehicle motion in (4.1) can be simplified as:

$$\begin{aligned} M_v \cdot \dot{v}_x &= F_{x,Ax1} + F_{x,Ax2} \approx F_{x,req} \\ M_v \cdot (v_x \cdot \omega_z) &= F_{y,Ax1} + F_{y,Ax2} \end{aligned} \tag{4.2}$$

Furthermore, a virtual lateral acceleration input can be used to introduce the

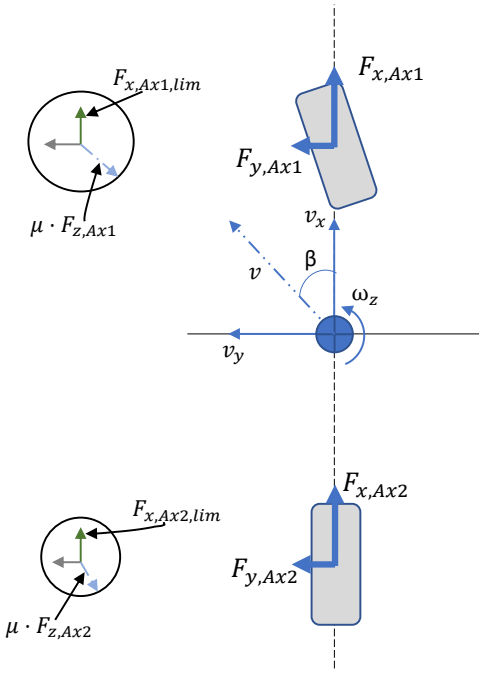

Figure 4.2: Single track vehicle model in the road plane having longitudinal, lateral and yaw rotational degree of freedom. The wheel forces on an axle are lumped into one axle force. In the left figure, the maximum wheel force limits of the axles drawn as circles and force vectors are calculated using vertical load, road friction and lateral force.

lateral forces on the axle, without using any steering actuator input or dynamics. Thus, using the lateral acceleration input and static load distribution, the total lateral force produced by each axle can be calculated. This is the minimum representation of the vehicle needed to study the axle coordination without adding extra effects of dynamics and actuator inputs. The lateral force on the axles, F_{yAx1}

and F_{yAx2}, can be calculated using static load distributions, F_{zAx1} and F_{zAx2} on the axles using (4.3).

$$\begin{aligned} F_{y,Ax1} &= F_{y,c1} + F_{y,c2} = \frac{M_v \cdot l_r \cdot g}{l_f + l_r} \cdot (v_x \cdot \omega_z) \\ F_{y,Ax2} &= F_{y,c3} + F_{y,c4} = \frac{M_v \cdot l_f \cdot g}{l_f + l_r} \cdot (v_x \cdot \omega_z) \\ \text{where, } &\frac{M_v \cdot l_r \cdot g}{l_f + l_r} = F_{z,Ax1} \text{ and } \frac{M_v \cdot l_f \cdot g}{l_f + l_r} = F_{z,Ax2} \end{aligned} \tag{4.3}$$

Depending on the vehicle configuration and e-axle topology, the forces from the actuators are different. Now, using the assumptions, (4.2) and (4.3), the constraints needed to fulfill the axle level coordination, used in the actuator coordination, can expressed in the general form as:

$$\sum_{i=1}^{m} \sum_{j=1}^{n_i} (F_{x,EMij,req} + F_{x,brkij,req}) = F_{x,req} \tag{4.4}$$

$i \in \{1....m\}$, Axle number
$j \in \{1..p_i..n_i\}$, where $(1..p_i)$ are EMs and $(p_i + 1..n_i)$ are friction brakes connected to an axle i.

For one axle, when $i = 1$: (4.5)

$$-F_{x,Ax1,lim} \leq \sum_{j=1}^{n_i} (F_{x,EM1j,req} + F_{x,brk1j,req}) \leq F_{x,Ax1,lim} \tag{4.6}$$

$$F_{x,Axi,lim} = \sqrt{(\mu \cdot F_{z,Axi})^2 - (F_{y,Axi})^2} \tag{4.7}$$

where, $\mu \cdot F_{z,Axi}$ is the maximum wheel force limit and $F_{x,Axi,lim}$, is the longitudinal wheel force limit of the axle.

Similarly for an axle i:

$$-F_{x,Axi,lim} \leq \sum_{j=1}^{n_i} (F_{x,EMij,req} + F_{x,brkij,req}) \leq F_{x,Axi,lim} \tag{4.8}$$

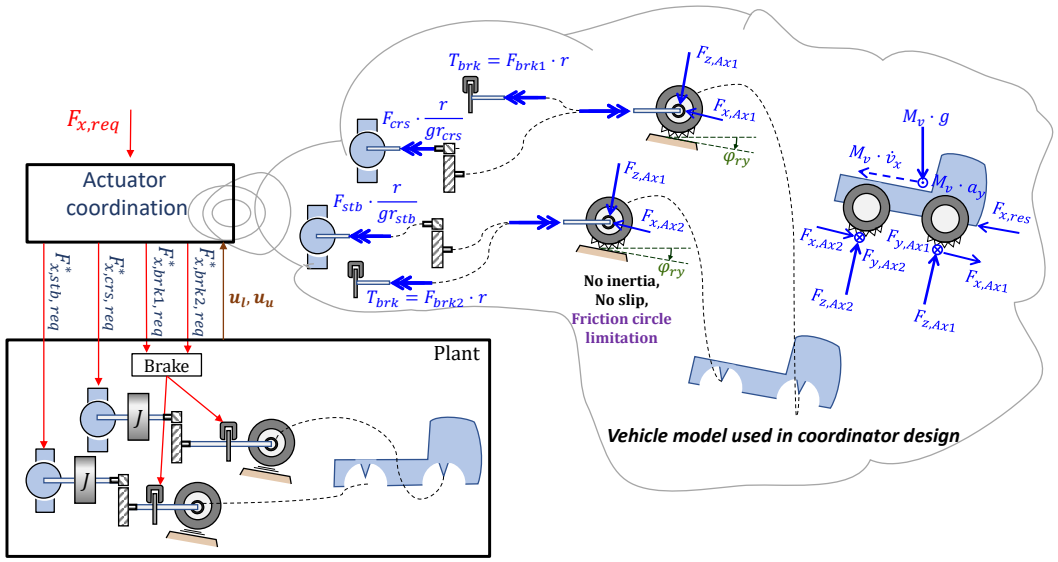

Figure 4.3: Pictorial abstract of the actuator coordination by adding axle constraints for a 4x4 vehicle configuration with cruise and startability axles. The vehicle model is represented as a two axle model in the actuator coordinator design.

4.3 Axle and actuator coordination of the topologies

The problem formulation to minimise power losses by adopting the axle constraints (4.8) in the actuator coordination formulation (3.3), for different powertrain topologies is generalised as the follows:

$$\begin{aligned} \boldsymbol{u}^* = \arg\min_{\boldsymbol{u}} \quad & \sum (P_{loss,EMij} + P_{loss,brkij}) \\ \text{s.t.} \quad & \boldsymbol{u_l} \leq \boldsymbol{u} \leq \boldsymbol{u_u} \\ & B \cdot \boldsymbol{u} = \boldsymbol{v} \\ & -\boldsymbol{h} \leq G \cdot \boldsymbol{u} \leq \boldsymbol{h} \end{aligned} \tag{4.9}$$

where,

$B \in \mathbb{R}^{(1 \times n_i)}$; $B(j) = 1$

$G \in \mathbb{R}^{(2m \times q_i)}$, where $q_i = max(n_i)$; $G(i,j) \in \{-1, 0, 1\}$

Matrix G, depends on the powertrain topology and vehicle configuration.

Refer subections 4.3.1 and 4.3.2 for implementation of G.

$$\boldsymbol{v} = F_{x,req} \tag{4.10}$$

$$\boldsymbol{h} = \left[F_{x,Ax1,lim}, \quad \ldots, F_{x,Axj,lim}, \quad \ldots, F_{x,Ax1,lim}, \quad \ldots, F_{x,Axj,lim}\right]^T \tag{4.11}$$

$$\boldsymbol{u} = \left[F_{x,EM11,req}, \quad \ldots, F_{x,EMmn,req}, F_{x,brk11,req}, \quad \ldots, F_{x,brkmn,req}\right]^T \tag{4.12}$$

$$\boldsymbol{u_l} = \left[F_{x,EM11,min}, \quad \ldots, F_{x,EMmn,min}, F_{x,brk11,min}, \quad \ldots, F_{x,brkmn,min}\right]^T \tag{4.13}$$

$$\boldsymbol{u_u} = \left[F_{x,EM11,max}, \quad \ldots, F_{x,EMmn,max}, F_{x,brk11,max}, \quad \ldots, F_{x,brkmn,max}\right]^T \tag{4.14}$$

Using (4.9)-(4.14), the axle and actuator coordination for different topologies are formulated. Figure 4.3, highlights the vehicle model representation used in the actuator coordination with axle constraints. In comparison with (3.3), the friction circle limits are included for wheels in addition to the vehicle model with two axles.

4.3.1 Single e-axle group

Axle coordination using power loss minimisation (SEP)

To evaluate the axle and actuator coordination algorithm for the single e-axle group topology, a 4x2 vehicle configuration is chosen. To compare the performance and power loss minimisation possible against the multiple e-axle groups, the same configuration of EMs, gear ratios, and friction brakes are chosen. This means that the two electric machines with respective gear ratios are connected to the wheels through a common shaft. Here, the gear ratio refers to the total ratio between the electric machine and the wheel. This also infers that the regeneration capability is limited to the rear axle only. Each wheel is equipped with its own friction brake actuator.

$$\begin{aligned} \boldsymbol{u^*} = \arg\min_{\boldsymbol{u}} \quad & (P_{loss,EM21} + P_{loss,EM22} + P_{loss,brk11} + P_{loss,brk21}) \\ \text{s.t.} \quad & \boldsymbol{u_l} \leq \boldsymbol{u} \leq \boldsymbol{u_u} \\ & B \cdot \boldsymbol{u} = \boldsymbol{v} \\ & -\boldsymbol{h} \leq G \cdot \boldsymbol{u} \leq \boldsymbol{h} \end{aligned} \tag{4.15}$$

$$\text{where} \quad B = \begin{bmatrix} 1 & 1 & 1 & 1 \end{bmatrix}, \quad G = \begin{bmatrix} 0 & 0 & -1 & 0 \\ -1 & -1 & 0 & -1 \\ 0 & 0 & 1 & 0 \\ 1 & 1 & 0 & 1 \end{bmatrix}$$

$$\boldsymbol{v} = F_{x,req}, \quad h = \left[F_{x,Ax1,lim}, F_{x,Ax2,lim}, F_{x,Ax1,lim}, F_{x,Ax2,lim}\right]^T$$

$$\boldsymbol{u} = \left[F_{x,EM21,req}, \quad F_{x,EM22,req}, \quad F_{x,brk11,req}, \quad F_{x,brk21,req}\right]^T$$

$$\boldsymbol{u_l} = \left[F_{x,EM21,min}, \quad F_{x,EM22,min}, \quad F_{x,brk11,min}, \quad F_{x,brk21,min}\right]^T$$

$$\boldsymbol{u_u} = \left[F_{x,EM21,max}, \quad F_{x,EM22,max}, \quad F_{x,brk11,max}, \quad F_{x,brk21,max}\right]^T$$

4.3.2 Multiple e-axle group

Axle coordination using power loss minimisation (MEP)

In the multiple e-axle group topology, the 4x2 vehicle in the **SEP** is configured as a 4x4. The powertrain is configured as the cruise and startability axles concept, with an EM and friction brake each, on both the front and rear axle. The axle and actuator coordination for multiple e-axle groups is formulated as the follows:

$$\begin{aligned} \boldsymbol{u}^* = \quad & \min_{\boldsymbol{u}} \ (P_{loss,EM11} + P_{loss,EM21} + P_{loss,brk11} + P_{loss,brk21}) \\ \text{s.t.} \quad & \boldsymbol{u_l} \leq \boldsymbol{u} \leq \boldsymbol{u_u} \\ & B \cdot \boldsymbol{u} = \boldsymbol{v} \\ & -\boldsymbol{h} \leq G \cdot \boldsymbol{u} \leq \boldsymbol{h} \end{aligned} \tag{4.16}$$

$$\text{where} \quad B = \begin{bmatrix} 1 & 1 & 1 & 1 \end{bmatrix}, \quad G = \begin{bmatrix} -1 & 0 & -1 & 0 \\ 0 & -1 & 0 & -1 \\ 1 & 0 & 1 & 0 \\ 0 & 1 & 0 & 1 \end{bmatrix}$$

$$\boldsymbol{v} = F_{x,req}, \quad h = \begin{bmatrix} F_{x,Ax1,lim}, F_{x,Ax2,lim}, F_{x,Ax1,lim}, F_{x,Ax2,lim} \end{bmatrix}^T$$
$$\boldsymbol{u} = \begin{bmatrix} F_{x,EM11,req}, & F_{x,EM21,req}, & F_{x,brk11,req}, & F_{x,brk21,req} \end{bmatrix}^T$$
$$\boldsymbol{u_l} = \begin{bmatrix} F_{x,EM11,min}, & F_{x,EM21,min}, & F_{x,brk11,min}, & F_{x,brk21,min} \end{bmatrix}^T$$
$$\boldsymbol{u_u} = \begin{bmatrix} F_{x,EM11,max}, & F_{x,EM21,max}, & F_{x,brk11,max}, & F_{x,brk21,max} \end{bmatrix}^T$$

As seen the only difference between the **SEP** and **MEP**, is the G matrix, $\boldsymbol{u}$, $\boldsymbol{u_l}$, and $\boldsymbol{u_u}$ that defines the powertrain topology assuming same actuators are used. As highlighted earlier having both $\boldsymbol{v}$ and $\boldsymbol{u}^*$ as force requests, simplifies the entries of G using 1´s and 0's.

Axle coordination using rule based allocation (MER)

To evaluate the effectiveness of the power loss minimisation algorithm, a rule-based allocation is implemented, using the multiple e-axle group topology.

An equal distribution strategy of force request is applied. This means that equal forces are applied on the front and rear axle actuators irrespective of wheel force limits. For deceleration requests, the EM usage are prioritised and used to their limits followed by friction brakes. The pseudocode of the rule-based allocation, assuming that the total force request does not exceed maximum wheel force limits, implemented is shown.

$$F_{x,Ax,lim} = \min(F_{x,Ax1,lim}, F_{x,Ax2,lim}) \tag{4.17}$$

Algorithm 1 Pseudo code to compute $\boldsymbol{u}^*$ based on $\boldsymbol{v}$

if $(\boldsymbol{v} < 0)$ and $(\boldsymbol{v} > (F_{x,EM11,min} + F_{x,EM21,min})$ **then**
$F_{x,EM11,req} = max(0.5 \cdot \boldsymbol{v}, (sign(\boldsymbol{v}) \cdot F_{x,Ax,lim}))$; $F_{x,EM21,req} = F_{x,EM11,req}$
$F_{x,brk11,req} = 0$; $F_{x,brk21,req} = 0$
else if $\boldsymbol{v} < (F_{x,EM11,min} + F_{x,EM21,min})$ **then**
$F_{x,EM11,req} = max(0.5 \cdot \boldsymbol{v}, (sign(\boldsymbol{v}) \cdot F_{x,Ax,lim}))$; $F_{x,EM21,req} = F_{x,EM11,req}$
$F_{x,brk11,req} = max(0.5 \cdot ((F_{x,EM11,min} + F_{x,EM21,min}) - \boldsymbol{v}), sign(\boldsymbol{v}) \cdot (F_{x,EM11,req} - F_{x,Ax,lim}))$; $F_{x,brk21,req} = F_{x,brk11,req}$
else
$F_{x,EM11,req} = (0.5 \cdot \boldsymbol{v})$; $F_{x,EM21,req} = (0.5 \cdot \boldsymbol{v})$
$F_{x,brk11,req} = 0$, $F_{x,brk21,req} = 0$
end if

$$\boldsymbol{u} = \begin{bmatrix} F_{x,EM11,req}, & F_{x,EM21,req}, & F_{x,brk11,req}, & F_{x,brk21,req} \end{bmatrix}^T$$
$$\boldsymbol{u_l} = \begin{bmatrix} F_{x,EM11,min}, & F_{x,EM21,min}, & F_{x,brk11,min}, & F_{x,brk21,min} \end{bmatrix}^T$$
$$\boldsymbol{u_u} = \begin{bmatrix} F_{x,EM11,max}, & F_{x,EM21,max}, & F_{x,brk11,max}, & F_{x,brk21,max} \end{bmatrix}^T$$

Chapter 5

Motion control by axle and actuator coordination

The driving range of a BEV is increased by minimising the losses of the actuators and distributing the requests between axles. The axle forces produced to achieve a motion request, depend on the topology, configuration, and control system of the powertrain. This chapter primarily presents the results of the actuator and axle coordination while minimising instantaneous power losses. In section 5.1, the methodology, inputs to produce the motion requests and configuration parameters are defined. The results from simulations are then analysed for the three formulations presented in chapter 4 and compared in section 5.2.

5.1 Methodology

To evaluate the performance of the axle and actuator coordination, a set of operating points, is used to exemplify the coordination. A vector of longitudinal vehicle speed, road gradient, longitudinal acceleration, lateral acceleration, and road friction co-efficient defines each operating point, see Table.5.1. Such quasi-steady state operating points are chosen to facilitate the conceptual comparisons of different topologies and optimisation algorithms. Besides, the powertrain topologies, the same powertrain configuration and vehicle parameters are used. For the **SEP** case, both the electric machines are connected to the rear axle. In the case of **MEP** and **MER**, the PMSM machines are connected to the front axle and IM to the rear axle. The common vehicle and powertrain configuration parameters used for evaluating the actuator coordination are seen in table 5.3 and 5.2 respectively. The parameters used represent an unladen tractor configuration. The operating points are so chosen, so as not to exceed the wheel force limits of either of the axles and the limits of the actuators. Figure 5.1, shows the schematic of

the axle and actuator coordination algorithm used for evaluation. The simulation model is developed in python-based development environment, and the power loss problem formulation is solved using the *quadprog* solver. The problem formula-

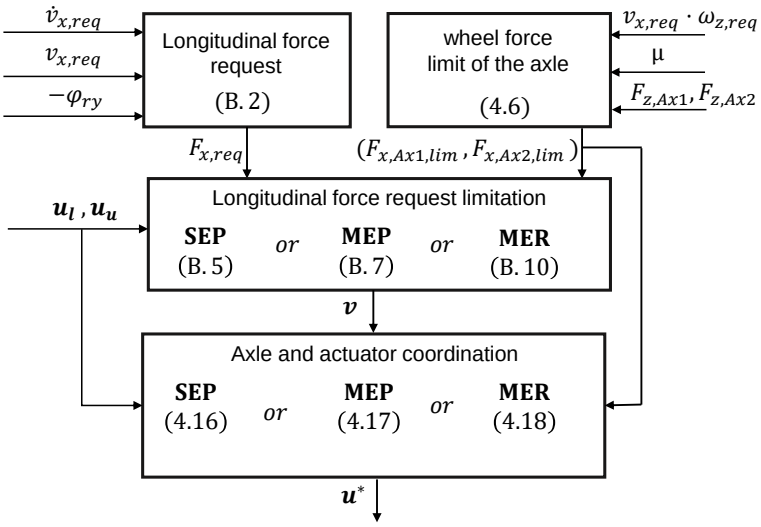

Figure 5.1: Schematic of axle and actuator coordination algorithm.

tions for axle and actuator coordination in chapter 4, of single and multiple e-axle group topologies are then calculated for different operating points. Results of axle and actuator coordination are used to compare the performance and limitations of different topologies. Additionally, the power loss associated with each operating point is also captured to evaluate the different topologies and coordination algorithms.

Table 5.1: Input parameters used to define the operating points.

Operating points	Input Parameters					Total force request, $F_{x,req}$ [kN]
	$v_x[m/s]$	$\varphi_{ry}[rad]$	$\dot{v}_x[m/s^2]$	$a_y \approx v_x \cdot \omega_z[m/s^2]$	μ	
OP_1	2.78	-0.05	1.48	0	0.7	18.00
OP_2	19.45	0.03	-2.45	0	0.5	-23.07
OP_3	13.89	0	-2.94	-2.94	0.6	-25.43
OP_4	11.11	0.02	-1.48	0.98	0.3	-14.18

Table 5.2: Powertrain configuration parameters

No. of electric machines	2
Configuration of the first electric machine	PMSM
Configuration of the second electric machine	IM
Max. continuous power of the PMSM [kW], $P_{max,crs}$	300
Max. rotational speed of the PMSM [rpm]	10000
Gear ratio coupled to PMSM, gr_{crs}	12
Max. continuous power of the IM [kW], $P_{max,stb}$	300
Max. rotational speed of the IM [rpm]	13000
Gear ratio coupled to IM, gr_{stb}	23

Table 5.3: Vehicle and environment parameters

Vehicle mass [kg], M_v	$9 \cdot 10^3$
Frontal area [m^2], A_v	9
Rolling resistance coefficient [-], C_r	0.005
Drag coefficient [-], C_d	0.59
Wheel radius [m], r	0.506
Air density [kg/m^3], ρ	1.2
Gravity constant [m/s^2], g	9.81
Max. continuous electric propulsion power [kW], P_{max}	600
Wheelbase [m], L	3.7
Longitudinal position of the front axle from CoG [m], l_f	1.32

5.2 Simulation results

The results from simulations per operating point for the problem formulations of **SEP**, **MEP** and **MER** are presented in this section. Figure 5.2-5.5, shows the coordinated axle force requests to achieve the total request for different operating points. The circles represent the maximum wheel force limit available for each axle . The green arrow represents the magnitude of the coordinated EM force and the red arrow represents the coordinated brake force, applied on an axle. Similarly, the lateral force on an axle depending on the lateral acceleration input is illustrated using the grey arrow. The maximum and minimum force limits of the EMs through the gear ratios available at the wheels are also plotted on each friction circle. These force limits are presented using horizontal orange and magenta lines for the front and rear axles, respectively. The brake force limits at the wheels are sufficiently high in magnitude and hence are excluded. The figures are complemented with coordinated values on each actuator per axle, using the tables 5.4-5.6 and thus can be used to verify the requested force for the operating points.

For $OP1$, as in figure 5.2, which represents taking-off at low speed on a uphill gradient and an accelerating vehicle, the requested force is fulfilled using the EMs. The maximum and minimum force limits of the EMs for the **SEP** case at $OP1$ are higher in magnitude than the wheel force limits on the rear axle. Nevertheless, any higher request than the maximum wheel force limits cannot be achieved for **SEP** case. In contrast, for the **MEP** and **MER** cases, there are some EM forces available to be used on both the axles before their limits. This means that with the multiple e-axle topology there is possibility to request more acceleration or ascend a higher gradient compared to the single e-axle topology for $OP1$. Furthermore, for the given powertrain configuration with the multiple e-axle topology, the maximum and minimum force limits of the EMs on the front axle are well within the maximum wheel force limits. This would also mean that there is some lateral force capability remaining on the front axle to handle steering requests. In comparison, the **SEP** has all of the maximum wheel force limits available to be used for the lateral forces on the front axles with no available force on the rear axles.

A decelerating vehicle moving down a gradient from high speed is described in $OP2$, and the results of the axle coordination is seen in figure 5.3. In the case of $OP1$ and $OP2$, the longitudinal wheel force limit is equal to the maximum wheel force limit of the axle. To achieve the force request for $OP2$, the **SEP** needs actuation of the friction brakes on the front axle. For the same request, the **MEP** and **MER** use only EMs. Tables 5.5 and 5.6, elucidate the differences in the axle coordination. This also means that **SEP** has the highest power loss compared to the other cases. In the case of **MEP** and **MER**, with a friction coefficient of 0.5,

the force limits on the front axle due to EMs are closer to the maximum wheel force limits than $OP1$, inferring reduced lateral force capabilities.

Both $OP3$ and $OP4$ represents cornering cases inducing lateral forces and thereby limiting the maximum available longitudinal force. $OP3$ an extreme situation of high deceleration while cornering with high lateral acceleration and $OP4$ represents a decelerating situation on ice while cornering. For **SEP** in $OP3$ and $OP4$, the deceleration is achieved using the combination of friction brake and EM. In comparison the multiple e-axle topology uses only EMs for $OP3$ and $OP4$. Tables 5.5 and 5.6, indicates the variation in the allocation of forces between the actuators. For $OP4$, the force limits due to EMs on the front axle, for **MEP** and **MER** cases, are on the maximum wheel force limit. This is undesirable, as higher force requests will reduce the lateral force capability on the front axle and affects the cornering behaviour of the vehicle significantly. However, for **MEP** and **MER**, there are still some lateral forces available to be used.

Finally, the power loss associated with each operating point for the three cases is presented in the table 5.7. To evaluate the total power loss, only electric machine and friction brake losses are included as in section 3.2. The load based losses due to gear tooth contact and other parasitic losses of the transmission are excluded in the calculation of power losses. This was done to avoid the complexities and details involved in the installation of different topologies. In the case of $OP1$, the **SEP** and **MEP** cases have the same magnitude of the power loss compared to **MER**. This shows that the power loss minimisation algorithm gives the lowest loss compared to the rule-based method. For the remaining operating points, the **MEP** case gives the minimum power loss, followed by the **MER** and then **SEP**. In the case of $OP2$, $OP3$ and $OP4$, the **SEP** case have significant power loss compared to the other cases. This is because of friction brakes being used to achieve the force request, as the rear axle force capability is saturated. Similarly, the rule-based coordination of **MER** also has higher power losses compared to the **MEP**. This difference in power loss is because of the optimal usage of EMs in **MEP**, minimising power losses for the given vehicle speed compared to **MER**.

Operating points	Front axle actuators [kN]	Rear axle actuators [kN]		
	$F_{x11,Brk}$	$F_{x21,EM}$	$F_{x22,EM}$	$F_{x21,Brk}$
OP_1	0	9.79	8.21	0
OP_2	-7.32	-13.7	-2.04	0
OP_3	-9.06	-6.58	-9.78	0
OP_4	-5.27	-4.85	-4.06	0

Table 5.4: Results of actuator coordination with **SEP** for the operating points.

Operating points	Front axle actuators [kN]		Rear axle actuators [kN]	
	$F_{x11,EM}$	$F_{x11,Brk}$	$F_{x21,EM}$	$F_{x21,Brk}$
OP_1	9.79	0	8.21	0
OP_2	-15.43	0	-7.64	0
OP_3	-10.23	0	-15.20	0
OP_4	-7.70	0	-6.47	0

Table 5.5: Results of actuator coordination with **MEP** for the operating points.

Operating points	Front axle actuators [kN]		Rear axle actuators [kN]	
	$F_{x21,EM}$	$F_{x21,Brk}$	$F_{x11,EM}$	$F_{x11,Brk}$
OP_1	9.00	0	9.00	0
OP_2	-11.53	0	-11.53	0
OP_3	-12.72	0	-12.72	0
OP_4	-7.08	0	-7.08	0

Table 5.6: Results of actuator coordination with **MER** for the operating points.

Operating points	Power loss [kW]		
	SEP	**MEP**	**MER**
OP_1	6.39	6.39	6.42
OP_2	155.26	17.85	22.72
OP_3	134.98	13.05	13.32
OP_4	67.45	10.65	10.68

Table 5.7: Total power loss of the EMs and friction brakes for the different operating points.

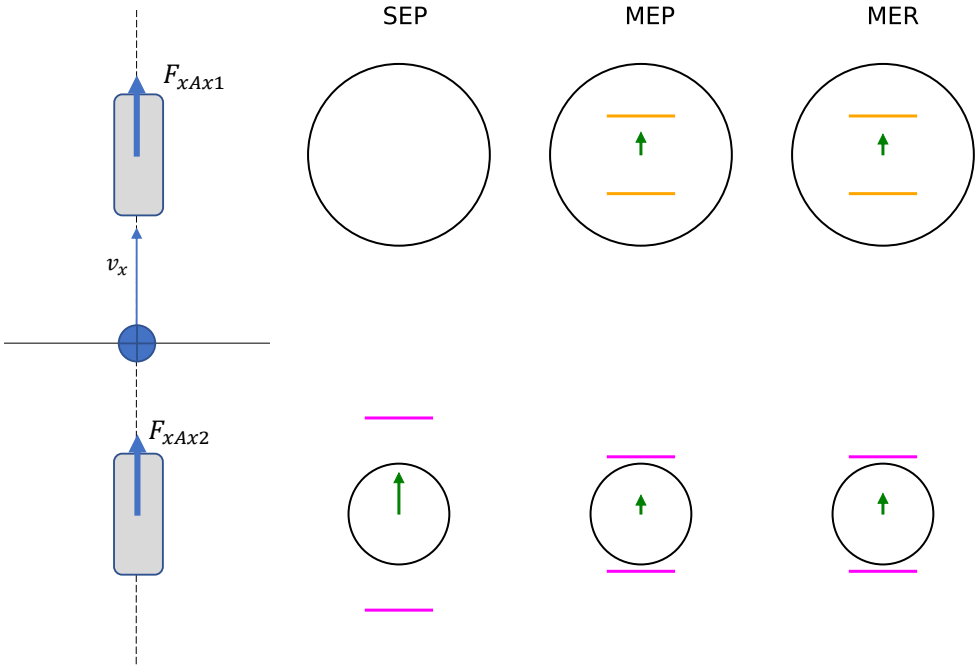

Figure 5.2: Axle force coordination for OP1.

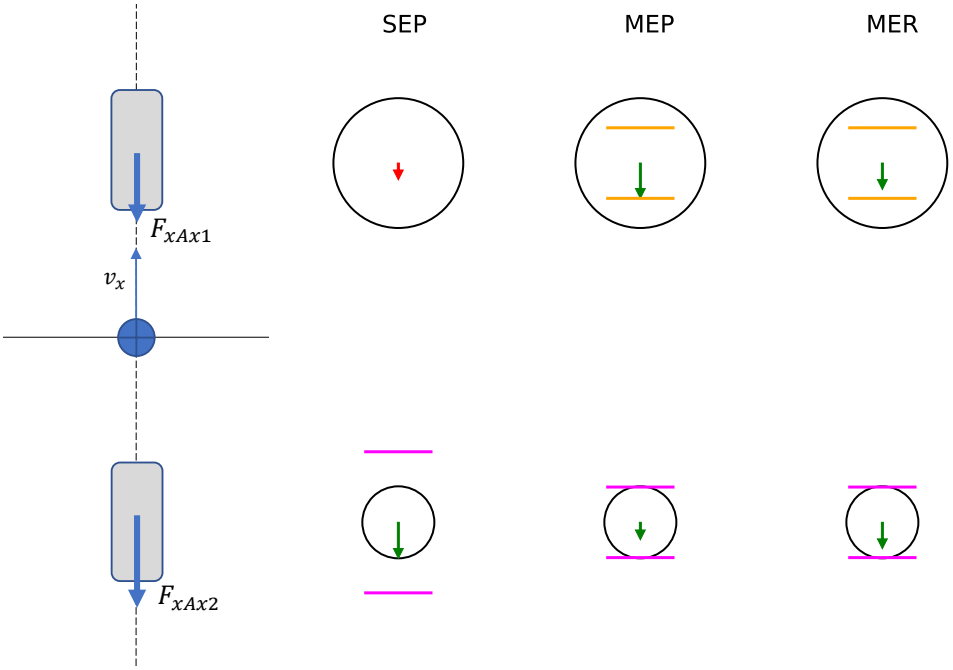

Figure 5.3: Axle force coordination for OP2.

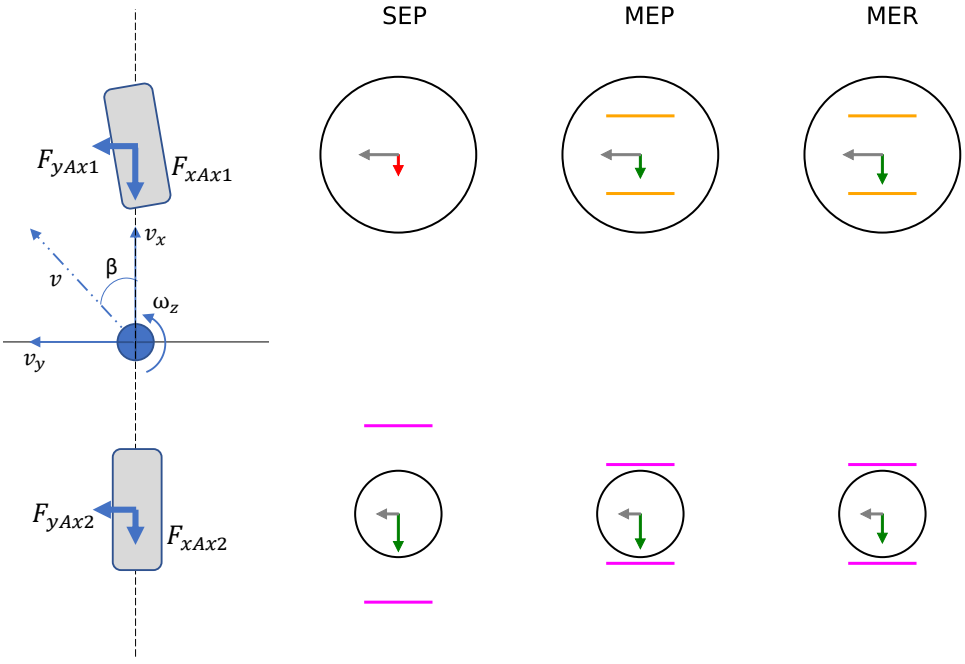

Figure 5.4: Axle force coordination for OP3.

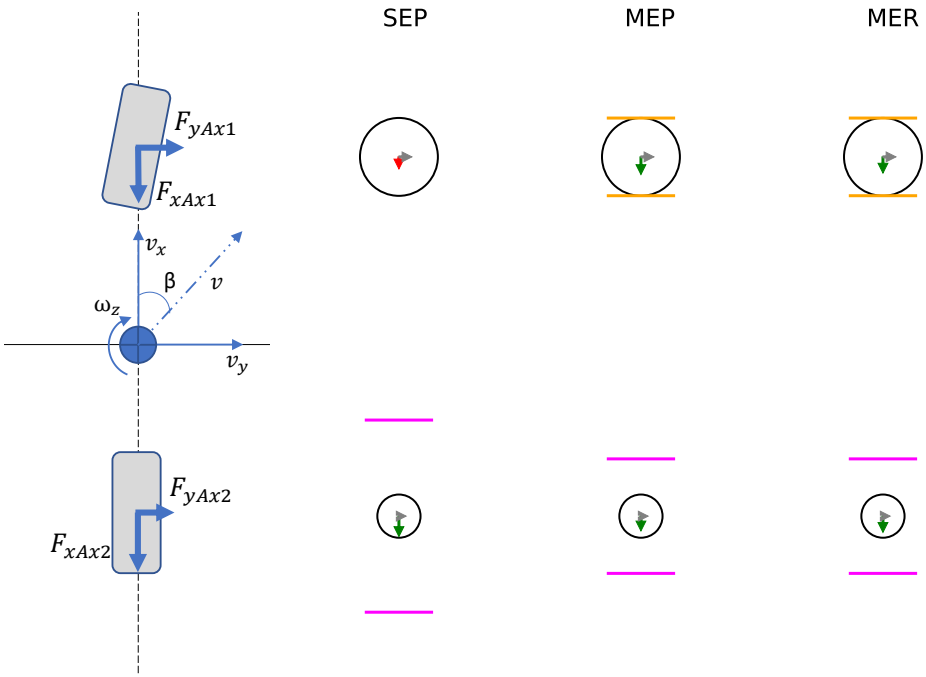

Figure 5.5: Axle force coordination for OP4.

Chapter 6

Conclusion and Future work

6.1 Conclusion

To increase the driving range of BEVs, the instantaneous losses must be minimised, while achieving the driver request or request from automatic driving algorithm, e.g. cruise controllers. By exploiting the motoring and generator capabilities, high power densities and cost-neutral scalability, of the electric machines, the potential of minimisation of power losses are explored. To analyse this potential, two electric powertrain topologies for BEVs are analysed namely, single e-axle group and multiple e-axle group. The multiple e-axle topology, using two different types of axle configurations namely cruise and startability axles is also presented.

To evaluate the performance of the cruise and startability axle concept, two different optimisation based control allocation methods of actuator coordination are introduced. A simulation model that receives longitudinal driver requests in terms of total force requests and operating limits of the actuators is used as an input. The same interfaces are used for the two optimisation methods. The first method is called power loss minimisation and uses physical models of actuator power losses as quadratic and linear functions. This optimisation problem formulation is then reformulated as a standard quadratic programming problem, which can be solved using numerical solvers. The second method called the weighted optimisation method, reduces the error between the total force request and actuator requests, rather than following the exact total force request. The weighted optimisation method is based on heuristic information of the system, such as efficient actuators, and involves tuning of actuator prioritisation. Such a method becomes complex when the number of actuators increases.

The power loss minimisation method is then extended by adding wheel force limits into the problem formulation. The wheel force limits are introduced using friction circle representation, thereby accounting the total available lateral and

longitudinal forces. This representation is added as constraints in the optimisation problem and thereby limiting the actuator coordination based within axle force saturation. This implementation is then verified on a single e-axle and multiple e-axle topologies for different force requests. An additional rule-based axle coordination is also developed to compare the performance with the power loss minimisation algorithm.

The results demonstrate the implementation of the powertrain topologies and power loss minimisation algorithm as expected. The following conclusions can be made using the results:

- **MEP** can achieve higher acceleration and deceleration with minimal losses, as seen in $OP1$ and $OP2$.
- **SEP** gives the highest power losses as observed at $OP2$-$OP4$. The difference in power loss **SEP** and **MEP** vary between 3 and 20 % depending on the operating condition.
- The difference between **MEP** and **MER** is not that significant. For $OP2$, **MER** has higher losses.
- The choice of powertrain topology has a significant influence on power losses than the actuator coordination method.

6.2 Future work

The following ideas are seen as a natural extension to the scope and limitations that were considered in this thesis:

- **System modelling and simulations:** In this thesis, lot simplifications and assumptions are made for the conceptual analysis of the topologies. This was necessary as such concepts do not currently exist as real BEVs or are under development. The wheel and powertrain dynamics used are greatly simplified and exclude effects such as inertia, wheel slip, and steering, etc. Moreover, only quasi-steady state cases are calculated with the focus on the actuator coordination in the longitudinal direction. The addition of controllers, vehicle plant and closing the loop for simulations is a logical step forward. These additions are expected to influence the force requests generated, actuator coordination formulation, and results. Hence, high-fidelity vehicle model with ample details are expected to improve the accuracy and validity of the results.

- **Additional sources of Power losses and TCO analysis:** The scope of this thesis was limited to the conceptual analysis of the actuator coordination for two types of powertrain topologies. No detailed comparison on the energy consumed for the topologies are performed. This requires a thorough and detailed modelling of the system including power losses of different systems and phenomenon, which are excluded in this thesis. For example, power losses due to tyre slip, rolling resistance, transmission, batteries, pneumatic and hydraulic systems needs to be included for an holistic analysis of the topologies. Such detailed modelling of the power losses encourages a thorough TCO comparison of the topologies and is a scope for future work.

- **Predictive energy strategies:** Predictive control is not included and neither are the losses from cooling and battery management systems considered in defining the actuator coordination. The motion request prepared is isolated from the overall energy consumption of the vehicle motion in an environment. Adding an interface to consider predictive control strategies or input from higher functional layers is expected to produce higher energy saving potential.

- **Electrical propulsion system modelling:** The electrical propulsion systems are simplified into simple models and lookup tables for the power loss minimisation algorithm. As highlighted, the possibility to de-energise IMs needs detailed modelling and investigation. This is related to the limitation of standard quadratic optimisation not accepting boolean requests and needs extension. An analysis and real vehicle testing using mixed integer quadratic programming is seen relevant for actuator coordination.

Appendix A

Formulation of mixed optimisation based control allocation as a standard quadratic programming problem

The control allocation (CA) problem as in (A.1) is rewritten as a quadratic programming (QP) formulation as shown in (A.8).

$$\begin{aligned} &\boldsymbol{u^*} = \text{argmin } \|W_u(\boldsymbol{u_{des}} - \boldsymbol{u})\|_2 + \gamma\|W_v(B\boldsymbol{u} - \boldsymbol{v})\|_2 \\ &\text{subject to } \ \boldsymbol{u_l} \leq \boldsymbol{u} \leq \boldsymbol{u_u} \end{aligned} \tag{A.1}$$

Rewriting and expanding the CA form (only the cost function) in (A.1).

Expansion of the actuator coordination term:

$$\begin{aligned} &\|W_u(u - u_d)\|_2^2 = (W_u(u - u_d))^T(W_u(u - u_d)) \\ &= (u^T - u_d^T)W_u^T W_u(u - u_d) \\ &= u^T W_u^T W_u u - u^T W_u^T W_u u_d - u_d^T W_u^T W_u u + u_d^T W_u^T W_u u_d \end{aligned} \tag{A.2}$$

$$\approx u^T W_u^T W_u u - 2u_d^T W_u^T W_u u + C1 \tag{A.3}$$

Similarly expansion of virtual control input coordination term yields:

$$\begin{aligned} &\|W_v(Bu - v)\|_2^2 = (W_v(Bu - v))^T(W_v(Bu - v)) \\ &= (u^T B^T - v^T)W_v^T W_v(Bu - v) \end{aligned}$$

$$= u^T B^T W_v^T W_v B u - u^T B^T W_v^T W_v v - v^T W_v^T W_v B u + v^T W_v^T W_v v \tag{A.4}$$

$$\approx u^T B^T W_v^T W_v B u - 2 v^T W_v^T W_v B u + C2 \tag{A.5}$$

Collecting and simplifying of terms from (A.3) and (A.5):

$$\begin{aligned} &\|W_u(u - u_d)\|_2^2 + \gamma \|W_v(Bu - v)\|_2^2 \\ &= u^T (W_u^T W_u + \gamma B^T W_v^T W_v B) u + C1 + C2 \\ &- 2(u_d^T W_u^T W_u + v^T W_v^T W_v B) u \end{aligned} \tag{A.6}$$

Comparing the terms in (A.3) and in (A.6), we could identify that,

$$\begin{aligned} H &= 2(W_u^T W_u + \gamma B^T W_v^T W_v B) \\ g^T &= -2(\boldsymbol{u_d}^T W_u^T W_u + \gamma \boldsymbol{v}^T W_v^T W_v B) \end{aligned} \tag{A.7}$$

These terms can be used to solve the QP problem as in (A.8).

$$\begin{aligned} \Longrightarrow \min_{\boldsymbol{u}} \quad & \frac{1}{2} \boldsymbol{u}^T H \boldsymbol{u} + g^T \boldsymbol{u} \\ \text{subject to} \quad & \boldsymbol{u}_l \leq \boldsymbol{u} \leq \boldsymbol{u}_u \\ & G\boldsymbol{u} \leq H \\ & A\boldsymbol{u} = B \end{aligned} \tag{A.8}$$

Appendix B

Longitudinal force request calculation and limitation

$$F_{x,req} = M_v \cdot \dot{v}_x + F_{x,res} \tag{B.1}$$

$$F_{x,res} = \frac{1}{2} \cdot \rho \cdot C_d \cdot A_v \cdot v_{x,req}^2 + M_v \cdot g \cdot (C_r + \sin(-\varphi_{ry})) \tag{B.2}$$

B.1 Limitation used in actuator coordination:

$$\boldsymbol{v} = \begin{cases} \max(F_{x,req}, \sum \boldsymbol{u_l}), & \text{if } F_{x,req} < 0 \\ \min(F_{x,req}, \sum \boldsymbol{u_u}), & \text{otherwise} \end{cases} \tag{B.3}$$

B.2 Limitation used in axle and actuator coordination:

B.2.1 SEP

$$F_{x,req,lim} = \begin{cases} \max(F_{x,req}, -(F_{xAx1,lim} + F_{xAx2,lim})), & \text{if } F_{x,req} < 0 \\ \min(F_{x,req}, F_{xAx2,lim}), & \text{otherwise} \end{cases} \tag{B.4}$$

$$\boldsymbol{v} = \begin{cases} \max(F_{x,req,lim}, \sum \boldsymbol{u_l}), & \text{if } F_{x,req,lim} < 0 \\ \min(F_{x,req,lim}, \sum \boldsymbol{u_u}), & \text{otherwise} \end{cases} \tag{B.5}$$

B.2.2 MEP

$$F_{x,req,lim} = \begin{cases} \max(F_{x,req}, -(F_{x,Ax1,lim} + F_{x,Ax2,lim})), & \text{if } F_{x,req} < 0 \\ \min(F_{x,req}, (F_{x,Ax1,lim} + F_{x,Ax2,lim})), & \text{otherwise} \end{cases} \tag{B.6}$$

$$\boldsymbol{v} = \begin{cases} \max(F_{x,req,lim}, \sum \boldsymbol{u_l}), & \text{if } F_{x,req,lim} < 0 \\ \min(F_{x,req,lim}, \sum \boldsymbol{u_u}), & \text{otherwise} \end{cases} \tag{B.7}$$

B.2.3 MER

$$F_{xAx,lim} = \min(F_{xAx1,lim}, F_{xAx2,lim}) \tag{B.8}$$

$$F_{x,req,lim} = \begin{cases} \max(F_{x,req}, -\min((F_{xAx1,lim} + F_{x,Ax2,lim}), 2 \cdot F_{x,Ax,lim})), & \text{if } F_{x,req} < 0 \\ \min(F_{x,req}, \min((F_{xAx1,lim} + F_{x,Ax2,lim}), 2 \cdot F_{x,Ax,lim})), & \text{otherwise} \end{cases} \tag{B.9}$$

$$\boldsymbol{v} = \begin{cases} \max(F_{x,req,lim}, \sum \boldsymbol{u_l}), & \text{if } F_{x,req,lim} < 0 \\ \min(F_{x,req,lim}, \sum \boldsymbol{u_u}), & \text{otherwise} \end{cases} \tag{B.10}$$

This logic for **MER** does not cover all the range of inputs and is a simplification, which is represented here. Refer the python code for implementation and updates.

Appendix C

Additional Results

In this section, some additional results for the axle and actuator coordination with a fully laden tractor are presented. However, no trailer and coordination of the trailer actuator are considered in this evaluation. The vehicle is assumed to be loaded and producing the maximum vertical legal loads on the axles. The operating points used for this evaluation are seen in table C.1, which mainly shows cases with low friction. Similarly, the vehicle parameters changed compared to table 5.3 in seen in table C.2. The powertrain configuration parameters are kept the same as in table 5.2

Table C.1: Input parameters used to define the operating points.

Operating points	Input Parameters					Total force request, $F_{x,req}$ [kN]
	$v_x[m/s]$	$\varphi_{ry}[rad]$	$\dot{v}_x[m/s^2]$	$a_y \approx v_x \cdot \omega_z[m/s^2]$	μ	
$OP_{1,loaded}$	2.78	-0.05	1.48	0	0.4	36.00
$OP_{2,loaded}$	19.45	0.03	-2.45	0	0.3	-47.35
$OP_{3,loaded}$	13.89	0	-2.45	-2.94	0.4	-42.65
$OP_{4,loaded}$	11.11	0.02	-1.48	1.48	0.3	-28.75

Table C.2: Vehicle and environment parameters

Vehicle mass [kg], M_v	$18 \cdot 10^3$
Centre of gravity relative to front axle [m], l_f	2.15

Operating points	Front axle actuators [kN]	Rear axle actuators [kN]		
	$F_{x11,Brk}$	$F_{x21,EM}$	$F_{x22,EM}$	$F_{x21,Brk}$
$OP_{1,loaded}$	0	17	19	0
$OP_{2,loaded}$	−16.57	−15.43	−15.34	0
$OP_{3,loaded}$	−15.50	−10.92	−16.23	0
$OP_{4,loaded}$	−2	−14.5	−12.2	0

Table C.3: Results of actuator coordination with **SEP** for the operating points.

Operating points	Front axle actuators [kN]		Rear axle actuators [kN]	
	$F_{x11,EM}$	$F_{x11,Brk}$	$F_{x21,EM}$	$F_{x21,Brk}$
$OP_{1,loaded}$	17	0	19	0
$OP_{2,loaded}$	−15.43	−6.76	−15.43	−9.73
$OP_{3,loaded}$	−17	−2.03	−21.6	−2.03
$OP_{4,loaded}$	−15.63	0	−13.11	0

Table C.4: Results of actuator coordination with **MEP** for the operating points.

Operating points	Power loss [kW]	
	SEP	**MEP**
$OP_{1,loaded}$	20.53	20.53
$OP_{2,loaded}$	354.44	353.09
$OP_{3,loaded}$	229.3	78.21
$OP_{4,loaded}$	41.05	19.50

Table C.5: Total power loss of the EMs and serivce brakes for the operating points.

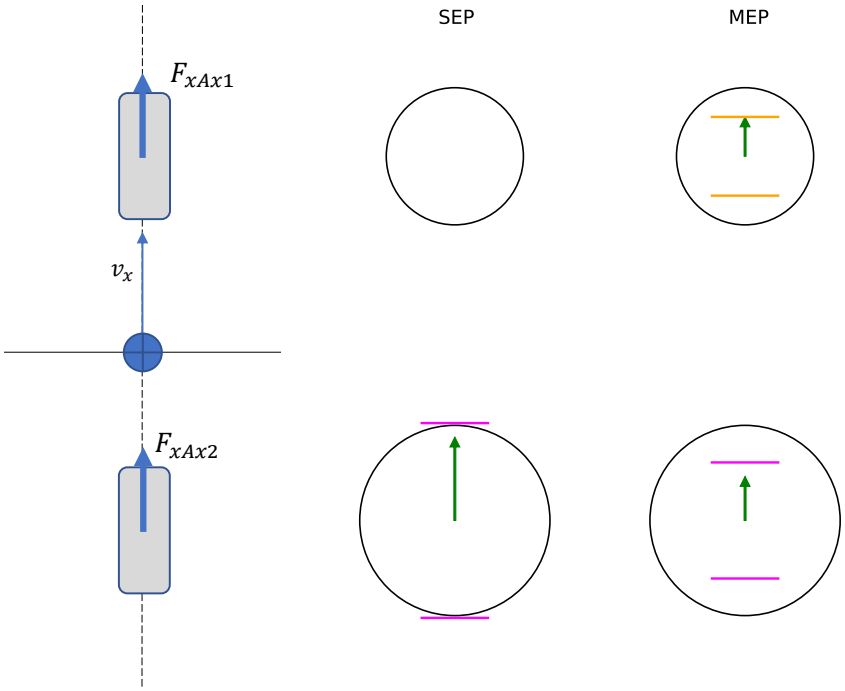

Figure C.1: Axle force coordination for loaded vehicle - $OP_{1,loaded}$.

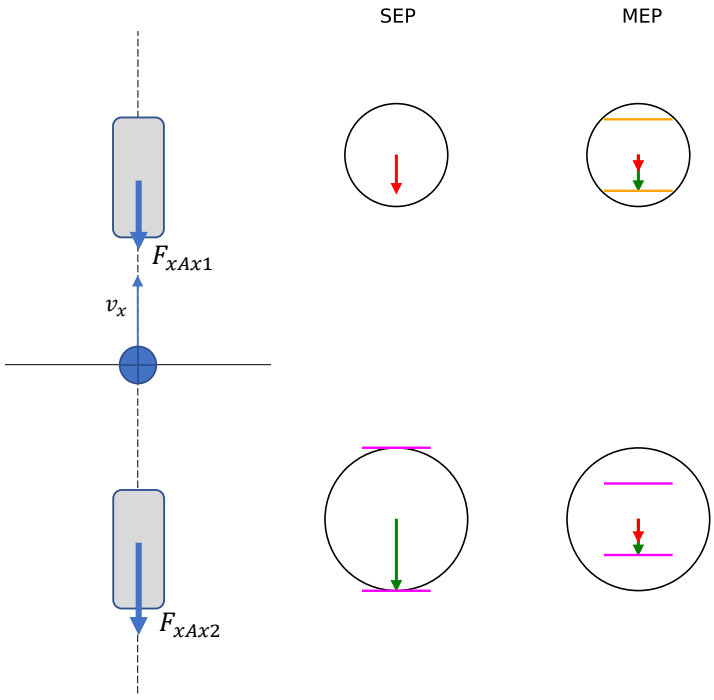

Figure C.2: Axle force coordination for $OP_{2,loaded}$. For the **MEP** case, the friction brakes are applied on top of the electric machines braking.

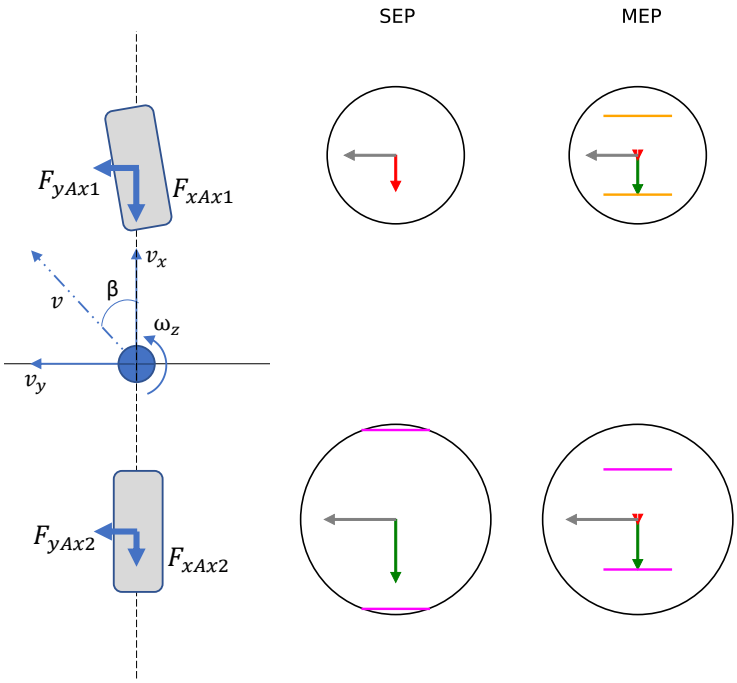

Figure C.3: Axle force coordination for $OP_{3,loaded}$.

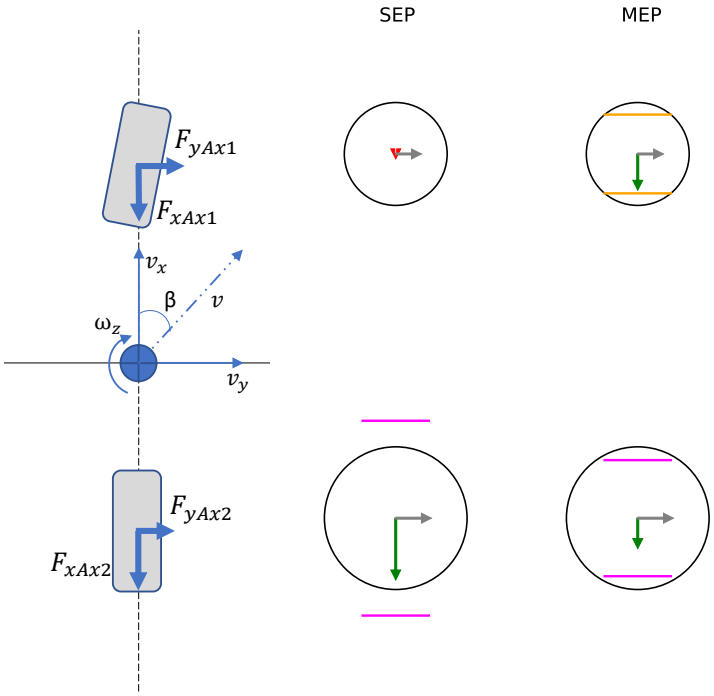

Figure C.4: Axle force coordination for $OP_{4,loaded}$.

Bibliography

[1] J. Andreasson, L. Laine, and J. Fredriksson, *Evaluation of a generic vehicle motion control architecture*, in Proceedings of World Automotive-Congress FISITA, 2004. QC 20100629.

[2] H. Basma, A. Saboori, and F. Rodríguez, *Total cost of ownership for tractor-trailers in europe: Battery electric versus diesel*, 2021.

[3] R. Basso, B. Kulcsár, B. Egardt, P. Lindroth, and I. Sanchez-Diaz, *Energy consumption estimation integrated into the electric vehicle routing problem*, Transportation Research Part D: Transport and Environment, 69 (2019), pp. 141–167.

[4] M. Bodson, *Evaluation of optimization methods for control allocation*, Journal of Guidance, Control, and Dynamics, 25 (2002), pp. 703–711.

[5] T. Bächle, K. Graichen, M. Buchholz, and K. Dietmayer, *Model predictive control allocation in electric vehicle drive trains*, IFAC-PapersOnLine, 48 (2015), pp. 335–340. 4th IFAC Workshop on Engine and Powertrain Control, Simulation and Modeling E-COSM 2015.

[6] DEWEsoft, *Current clamps and transducers tech specs, fluxgate ac/dc clamps*. Available online:"https://dewesoft.com/products/interfaces-and-sensors/current-clamps-and-transducers/tech-specs",(Accessed:Jan30,2023).

[7] Green car congress, *Daf trucks showcases electric and hybrid trucks at iaa cv*. Available online:"https://www.greencarcongress.com/2018/09/20180927-daf.html",(Accessed:Dec28,2022).

[8] T. Gundogdu, Z.-Q. Zhu, and C. C. Chan, *Comparative study of permanent magnet, conventional, and advanced induction machines for traction applications*, World Electric Vehicle Journal, 13 (2022).

[9] O. Härkegård, *Backstepping and control allocation with applications to flight control*, PhD thesis, Linköpings universitet, 2003.

[10] X. Hu, Y. Li, C. Lv, and Y. Liu, *Optimal energy management and sizing of a dual motor-driven electric powertrain*, IEEE Transactions on Power Electronics, 34 (2019), pp. 7489–7501.

[11] Insideevs, *Tesla semi: It's a beast with tri-motor system.* Available online:"https://insideevs.com/news/624742/tesla-semi-beast-tri-motor-system/",(Accessed:Jan27,2023).

[12] M. Jonasson, J. Andreasson, B. Jacobson, and A. S. Trigell, *Global force potential of over-actuated vehicles*, Vehicle System Dynamics, 48 (2010), pp. 983–998.

[13] KVASER, *The can bus protocol tutorial.* Available online:"https://www.kvaser.com/can-protocol-tutorial/",(Accessed:Jan30,2023).

[14] L. Laine, *Reconfigurable motion control systems for over-actuated road vehicles*, Chalmers University of Technology Göteborg, Sweden, 2007.

[15] Lohner–Porsche, *Lohner–porsche — Wikipedia, the free encyclopedia.* Available online:"https://en.wikipedia.org/wiki/Lohner%E2%80%93Porsche",(Accessed:Jan2,2023).

[16] E. mobility engineering, *Liebherr etm series.* Available online:"https://www.emobility-engineering.com/liebherr-etm-ev/",(Accessed:Jan23,2023).

[17] M. W. Oppenheimer, D. B. Doman, and M. A. Bolender, *Control allocation for over-actuated systems*, in 2006 14th Mediterranean Conference on Control and Automation, 2006, pp. 1–6.

[18] F. J. Oskar Dahl, *Understanding usage of volvo trucks*, Master's thesis, 2019.

[19] J. Torinsson, M. Jonasson, D. Yang, and B. Jacobson, *Energy reduction by power loss minimisation through wheel torque allocation in electric vehicles: a simulation-based approach*, Vehicle System Dynamics, 0 (2020), pp. 1–24.

[20] F. J. R. Verbruggen, E. Silvas, and T. Hofman, *Electric powertrain topology analysis and design for heavy-duty trucks*, Energies, 13 (2020).

[21] Volvo group, *Looking back – stories from the archive.* Available online:"https://images.volvotrucks.com/search?filtersStateId=11",(Accessed:Dec28,2022).

[22] VOLVO TRUCKS, *Volvo fh electric. from city to city in comfort.* Available online:"https://www.volvotrucks.com/en-en/trucks/trucks/volvo-fh/volvo-fh-electric.html",(AccessedJan27,2023).

Paper A

Concept design of electric cruise and startability axles for long haul heavy vehicles to maximise driving range

Paper B

Motion control and power coordination of electric propulsion and braking distributed on multiple axles on heavy vehicles

Paper C

Reviewing control allocation using quadratic programming for motion control and power coordination of battery electric vehicles